Chinese Journal of Aeronautics, (2026), 39(7): 104084

Chinese Society of Aeronautics and Astronautics
& Beihang University

Chinese Journal of Aeronautics

cja@buaa.edu.cn
www.sciencedirect.com

FULL LENGTH ARTICLE

A unified framework for multi-agent formation with a non-repetitive leader: Adaptive control and iterative learning control

Wei JIANG [a,b], **Yiyang CHEN** [b,*], **Hongtian CHEN** [c], **Bart De SCHUTTER** [d]

[a] *Department of Electrical Engineering and Automation, School of Electrical Engineering, Aalto University, Espoo, Finland*
[b] *School of Mechanical and Electrical Engineering, Soochow University, Suzhou 215137, China*
[c] *School of Automation and Intelligent Sensing, Shanghai Jiao Tong University, Shanghai 200240, China*
[d] *Delft Center for Systems and Control, Delft University of Technology, Delft, the Netherlands*

Received 8 August 2025; revised 11 September 2025; accepted 31 October 2025
Available online 21 January 2026

KEYWORDS

Adaptive observers;
Formation control;
Iterative learning control;
Multi-agent systems;
Unknown non-repetitive leader

Abstract Formation Tracking (FT) control is aimed at handling cooperative tasks in Multi-Agent Systems (MASs) to achieve desired performance. In these tasks, the leader's input is generally nonzero and unknown to all followers, i.e., its trajectory can be arbitrary and non-repetitive. In this paper, the additive property of linear systems is exploited to develop a unified framework for FT tasks of MASs, consisting of Adaptive Observer-based Control (AOC) and Iterative Learning Control (ILC). An AOC controller is employed to guarantee a fixed-shape formation between the leader and followers during the whole process, which reserves the initial condition for ILC. And ILC is used to improve the FT performance of certain repetitive tasks (followers rotating around the leader) over the trials. This gives rise to a fully distributed algorithm working for a directed communication graph containing a spanning tree without requiring any eigenvalue information from the Laplacian matrix of the graph, which enables its application to MASs with a large number of agents. Comparison is made via a numerical simulation to show that the proposed combined AOC-ILC algorithm has less FT error than pure AOC (without ILC), which validates the feasibility and efficacy of this algorithm.

1. Introduction

Research on cooperative distributed control of Multi-Agent Systems (MASs) has been carried out for more than two decades ranging from consensus, formation, containment, swarming, flocking and rendezvous, etc. In particular, formation control with applications in target enclosing, cooperative localization, load transportation by Unmanned Aerial Vehicles

* Corresponding author.
E-mail address: yychen90@suda.edu.cn (Y. CHEN).

☆ This article is part of a special issue entitled: 'Cooperative PD&C' published in Chinese Journal of Aeronautics.
Peer review under responsibility of Editorial Committee of CJA.

ELSEVIER Production and hosting by Elsevier

https://doi.org/10.1016/j.cja.2026.104084
1000-9361

(UAVs), seabed exploration by autonomous marine vehicles and so on. The work[1–5] has greatly captured the interest of researchers by some impressive work on consensus or synchronization control.[6,7] For a detailed overview of formation control, readers are referred to the research[8,9] and the references therein.

In general, there exist three types of formation scenarios: leaderless, virtual leader (a reference trajectory or an autonomous system without input), and real leader. Results associated to the former two scenarios, the solutions[10–15] have certain application limitations due to the following two reasons: (A) the followers have no idea where to go if the formation is leaderless; (B) the trajectory space of the followers is restricted as the virtual leader's trajectory is usually predefined and cannot be changed on-line. In the last scenario, the leader is real with a unicycle model,[16] with a constant velocity,[17] and general linear dynamics,[18,19] and is able to move anywhere it can by changing its input signal to follow a target or to avoid obstacles in real time. To deal with the real leader's non-zero input signal, inspired by sliding-mode control, a non-linear sliding-mode surface function which is state-dependent is usually utilized to compensate the effect of the non-zero input. Thus, a Formation Tracking (FT) error bound is generated.

To decrease this FT error bound in the real leader case, the authors propose a different point of view here: follower's trajectory. Although each follower's formation trajectory is generally non-repetitive, it can be considered as the sum of a non-repetitive trajectory and a repetitive trajectory. For example, a formation shape theory was proposed in which followers are required to rotate around the leader in a repetitive manner, i.e., relative to the leader, followers' trajectories are repetitive.[20] Because of the additive property of linear systems (linearity property), these two sub-trajectories (non-repetitive/repetitive) can be tracked using two independent input signals. To improve the performance of repetitive tasks, the technique of Iterative Learning Control (ILC) can be employed to iteratively update the input signal based on the learned past information.[21] Due to its learning mechanism, ILC can handle the repetitive aspects defined on time, space, or events. In this sense, it can be embedded into the formation control problem (where followers need to rotate around the real leader) to improve the repetitive tracking performance, i.e., to further reduce the FT error bound. Therefore, ILC is embedded in this paper along with a formation controller to handle the target of both repetitive and non-repetitive trajectory tracking.

The initial definition of ILC theory was given.[22] Then, several publications have contributed to the progress and applications of ILC in various areas, such as pick-and-place tasks,[23–26] wafer stages,[27] path planning,[28–31] process control,[32–34] and rehabilitation.[35] A brief literature review about ILC and formation control is presented next. The research[36] applied ILC to multi-agent formation for the first time. Subsequent work has further extended these results. However, there is no leader in some certain cases,[37] and the trajectories of the virtual leader are repetitive,[38,39] e.g., static or circles, due to the repetitive design requirement of ILC. Meanwhile, the controllers developed in these works require the knowledge of the whole communication graph (a piece of global information), so they are not fully distributed and might be hard to be applied to large-scale MASs due to the dramatically time-consuming calculation load. In addition, the iteration-varying formation shape mechanism during ILC trials is investigated.[40–42]

The link between formation control and ILC motivates to establish a unified framework using adaptive control and ILC. The design objective is to integrate Adaptive Observer-based Control (AOC) and ILC techniques to design a fully distributed AOC-ILC algorithm to realize FT control for general linear MASs with a non-repetitive leader. This framework does not require any global information and allows the real leader's trajectory to be arbitrary and non-repetitive, which extends the application area of ILC technique. Firstly, partially based on previous work,[12,20] the AOC controller (that can realize FT independently, herein called pure AOC) is further extended to the real leader case. Then, from the additive property of linear space in mathematics, instead of using AOC for FT directly, AOC is used to achieve the fixed-shape FT (shape translation performance), which also reserves the initial state condition for ILC at the beginning of each trial (the identical initial condition assumption for ILC is relieved). After that, the formation geometric shape theory is generalized and the ILC technique is adopted to fulfill the shape rotation performance. The overall input for each follower is the sum of its AOC and ILC controllers. There are mainly three contributions in this paper as follows:

(1) A unified framework is developed using AOC and ILC based on the additive property of linear space, which contributes to a novel FT mechanism. The proposed AOC-ILC controller is fully distributed (not require the communication graph information) and can decrease the FT error given a real leader with a non-zero input.
(2) This framework extends the ILC task description to allow a non-repetitive trajectory for a real leader with partially repetitive follower trajectories, which is different from a circle trajectory (repetitive) of the leader[38] or a static virtual leader/reference.[39]
(3) During each ILC trial, compared to a fixed formation shape (i.e., only shape translation)[36–39] or an iteration-varying formation shape,[40–42] the shape in this paper can be time-varying, i.e., shape translation and rotation are allowed simultaneously.

2. Preliminaries

2.1. Notation and graph theory

Throughout this paper, the basic notations and symbols of linear spaces and graph theory are organized into Table 1 for the convenience of readers. In addition, based on the definitions of the symbols in the table, related graph theory preliminaries are introduced below.

The matrix $\mathscr{A} = [a_{ij}] \in \mathbb{R}^{N\times N}$ is called a non-singular M-matrix if $a_{ij} \leqslant 0, \forall i \neq j$. The elements in adjacency matrix $\mathscr{A}$ are defined such that $[a_{ij}] = 1$ if $(j, i) \in \mathscr{E}$, and $a_{ij} = 0$ otherwise and all nodes that can transmit information to node i directly are said to be in-neighbors of node i and belong to the set $\mathscr{N}_i$. The elements in Laplacian matrix $\mathscr{L}$ are defined as $l_{ii} := \sum_{j\neq i} a_{ij}$ and $l_{ij} := -a_{ij}$ for all $i \neq j$. A directed path from node i to node j is a sequence of edges linking i to j. A directed graph (digraph) contains a directed spanning tree if there exists a node from which there is a directed path to every other node.

Table 1 Notation and symbol.

Symbol	Definition
$\mathbb{R}^n$	n-dimensional Euclidean space
$\mathbb{R}^{m\times n}$	Set of all $m \times n$ real matrices
$\mathbf{0}_{m\times n}$	$m \times n$ matrix with all entries being 0
$\mathbf{1}$	Column vector with all entries being 1
$\otimes$	Kronecker product
$\mathrm{diag}(a_1, a_2, \ldots, a_n)$	Diagonal matrix with $a_1, a_2, \ldots, a_n$ on the diagonal
$\boldsymbol{A} \succ 0$	$\boldsymbol{A}$ is symmetric and positive definite
$\lambda_{\min}(\boldsymbol{A})$	Minimal eigenvalue of $\boldsymbol{A}$
$\lambda_{\max}(\boldsymbol{A})$	Maximal eigenvalue of $\boldsymbol{A}$
$\parallel \boldsymbol{x} \parallel_\infty$	Infinity norm of vector $\boldsymbol{x}$
$\parallel \boldsymbol{x} \parallel$	2-norm of vector $\boldsymbol{x}$
$L_2^p[a,b]$	The space $\mathbb{R}^p$ valued Lebesgue square summable sequences on $[a,b]$
I_a^b	The set $\{a, a+1, ..., b\}$ for any integer $a \leqslant b$
$\mathscr{G} = (\mathscr{V}, \mathscr{E})$	Graph with vertex set $\mathscr{V}$ and edge set $\mathscr{E}$
$\mathscr{V} = \{1, 2, \ldots, N\}$	Finite non-empty set of nodes
$\mathscr{E} \subset \mathscr{V} \times \mathscr{V}$	Edge set of the graph
$\mathscr{A} = [a_{ij}] \in \mathbb{R}^{N\times N}$	Adjacency matrix
$\mathscr{N}_i = \{i \mid (j,i) \in \mathscr{E}\}$	i-th neighbor set of the graph
$\mathscr{L} = [l_{ij}] \in \mathbb{R}^{N\times N}$	Laplacian matrix

2.2. System model

The system dynamics of N followers as well as the leader indexed by 0 are described using the state space form as

$$\begin{cases} \dot{\boldsymbol{x}}_i(t) = \boldsymbol{A}\boldsymbol{x}_i(t) + \boldsymbol{B}\boldsymbol{u}_i(t) \\ \boldsymbol{y}_i(t) = \boldsymbol{C}\boldsymbol{x}_i(t), i \in I_0^N \end{cases} \tag{1}$$

where $\boldsymbol{x}_i(t) \in \mathbb{R}^n$, $\boldsymbol{u}_i(t) \in \mathbb{R}^p$, and $\boldsymbol{y}_i(t) \in \mathbb{R}^q$ are respectively the state, input, and measured output of the i-th agent, and where $\boldsymbol{A} \in \mathbb{R}^{n\times n}, \boldsymbol{B} \in \mathbb{R}^{n\times p}$ and $\boldsymbol{C} \in \mathbb{R}^{q\times n}$ are constant matrices. No follower needs to know the leader's input value.

The following assumptions are made in this paper to realize the control design objective.

Assumption 1. $(\boldsymbol{A}, \boldsymbol{B})$ is stabilizable. $(\boldsymbol{C}, \boldsymbol{A})$ is detectable.

Assumption 2. $\|u_0(t)\| \leqslant \delta$ where $\delta > 0$ is a constant.

Assumption 3. The directed graph $\mathscr{G}$ contains a spanning tree where the leader acts as the root node.

Then, the Laplacian matrix of the digraph $\mathscr{G}$ can be partitioned as $\mathscr{L} = \begin{bmatrix} \mathbf{0} & \mathbf{0}_{1\times N} \\ \mathscr{L}_2 & \mathscr{L}_1 \end{bmatrix}$, where $\mathscr{L}_1 \in \mathbb{R}^{N\times N}, \mathscr{L}_2 \in \mathbb{R}^{N\times 1}$. Under Assumption 3, all the eigenvalues of $\mathscr{L}_1$ have positive real parts. It is also easy to verify that $\mathscr{L}_1$ is a non-singular M-matrix.[43]

Denote $\boldsymbol{h}_i(t) \in \mathbb{R}^n$ as the relative vector from the leader to the follower i, i.e., the design target is to make $\boldsymbol{h}_i(t) = \boldsymbol{x}_i(t) - \boldsymbol{x}_0(t)$. If the vector $\boldsymbol{h}(t) = [\boldsymbol{h}_1^{\mathrm{T}}(t), \boldsymbol{h}_2^{\mathrm{T}}(t), \ldots, \boldsymbol{h}_N^{\mathrm{T}}(t)]^{\mathrm{T}}$ is piecewise continuously differentiable and time-varying, the multi-agent shape is time-varying.[11,12,20] Inspired by the work,[11] the authors[44,45] have proposed formation shapes that are complicated in mathematics and also, strict constraints have to be satisfied in their first priority. For instance, the research[45] assumes that the matrices $\boldsymbol{B} \in \mathbb{R}^{n\times p}$ and $\boldsymbol{C} \in \mathbb{R}^{q\times n}$ in Eq. (1) satisfy $\mathrm{rank}(\boldsymbol{B}) = p$ and $\mathrm{rank}(\boldsymbol{C}) = q$ such that there exist a non-singular matrix $\left[\bar{\boldsymbol{B}}^{\mathrm{T}}, \quad \tilde{\boldsymbol{B}}^{\mathrm{T}}\right]^{\mathrm{T}}$ with $\bar{\boldsymbol{B}} \in \mathbb{R}^{p\times n}$ and $\tilde{\boldsymbol{B}} \in \mathbb{R}^{(n-p)\times n}$, and a matrix $\bar{\boldsymbol{C}} \in \mathbb{R}^{n\times q}$ satisfying $\bar{\boldsymbol{B}}\boldsymbol{B} = \boldsymbol{I}_p$, $\tilde{\boldsymbol{B}}\boldsymbol{B} = 0$, $\boldsymbol{C}\bar{\boldsymbol{C}} = \boldsymbol{I}_q$. Then, the feasibility condition of the formation shape[45] is

$$\lim_{t\to\infty}(\tilde{\boldsymbol{B}}\boldsymbol{A}\bar{\boldsymbol{C}}\boldsymbol{h}_i(t) - \tilde{\boldsymbol{B}}\bar{\boldsymbol{C}}\dot{\boldsymbol{h}}_i(t)) = 0 \tag{2}$$

From a different point of view, the work[20] proposed a different formation shape format as

$$\dot{\boldsymbol{h}}_i(t) = (\boldsymbol{A} + \boldsymbol{B}\boldsymbol{K}_1)\boldsymbol{h}_i(t), i \in I_1^N \tag{3}$$

with $\boldsymbol{K}_1 \in \mathbb{R}^{p\times n}$ being a constant matrix to be decided. One can find out that compared to Eq. (2), the mathematical structure of Eq. (3) is simpler and easier to satisfy due to the freedom of designing $\boldsymbol{K}_1$. The shape Eq. (3) is thus utilized in this paper to construct the formation shape for MASs. For a better FT problem presentation flow, more detailed explanations of the shape Eq. (3) are presented in Section 4.2.1.

It is worth noting that all the above works involve either leaderless formation control[11] or leader–follower formation control with a virtual leader.[20] The real leader–follower formation control is investigated,[46] where the formation shape has a similar format as Eq. (2) and the FT error is bounded. In the next section, the FT problem will be formulated by the cooperation of AOC and ILC to further improve the FT performance, i.e., to have a smaller bounded FT error.

3. Solutions to FT problems based on AOC

3.1. Formation tracking problem formulation

As shown in Fig. 1, the FT controller design consists of two processes aiming at further improving FT performance in the real leader case.

Step 1. During the whole FT horizon, the followers are asked to follow a non-repetitive trajectory in the ground coordinate system.

Step 2. In addition, during the ILC trials $[t^k, \ t^k + T]$, each follower is expected to follow a repetitive trajectory around the leader in the leader coordinate system.

To be more specific, in Step 1, the non-repetitive trajectory can be, e.g., the shape translation from moment t_1 to t_2 as shown in Fig. 2. In Step 2, a repetitive trajectory around the leader could be rotating around the leader, i.e., following a closed-loop trajectory, e.g., a circle or an ellipse, as shown at moment t_2 in Fig. 2.

Note that k is the trial index as 0, 1, 2 and so on, t^k is the start time of the k-th trial, and T is the ILC trial length (the moment t^0 differs from the moment $t = 0$ s of the whole FT process).

As a result, the FT controller design resides on three key points: AOC, ILC and task description $\boldsymbol{h}_i(t)$. Note that $\boldsymbol{h}_i(t)$ can be designed by different tasks.

In this specific task design framework, the formation shape format $\boldsymbol{h}_i(t)$ can be split into two components as

$$\boldsymbol{h}_i(t) = \boldsymbol{h}_i^{\mathrm{aoc}}(t) + \boldsymbol{h}_i^{\mathrm{ilc}}(t), \ t \in [0, +\infty] \tag{4}$$

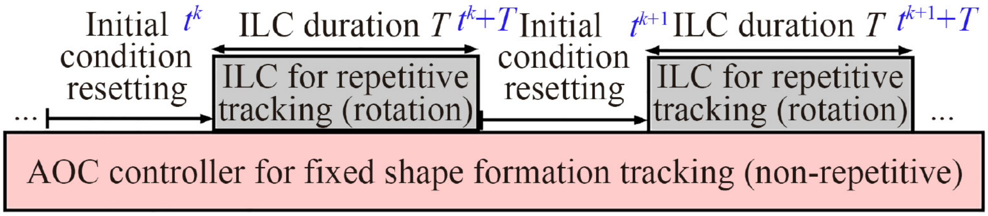

Fig. 1 An example of fully distributed controller algorithm construction: AOC and ILC workflow.

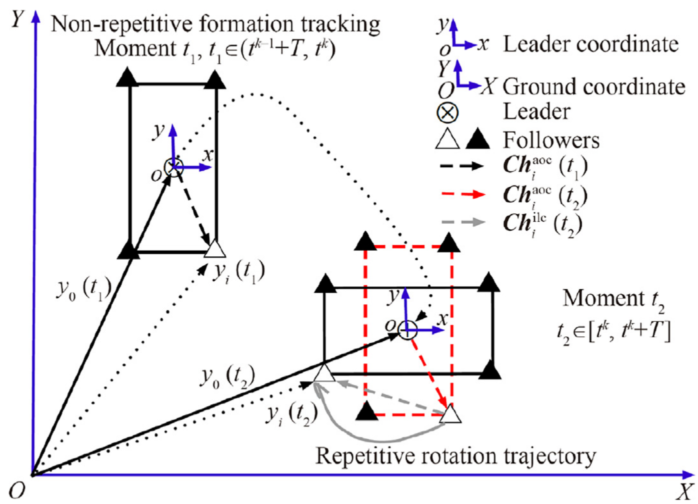

Fig. 2 Scenario of FT under ground coordinate and leader coordinate system.

where $\boldsymbol{h}_i^{\text{aoc}}(t)$ is a constant value over the FT horizon, and $\boldsymbol{Ch}_i^{\text{aoc}}(t)+\boldsymbol{y}_0(t)$ denotes the above mentioned non-repetitive trajectory in the ground coordinate system for follower i to track. The component $\boldsymbol{h}_i^{\text{ilc}}(t)$ is a time-varying repetitive value defined as

$$\boldsymbol{h}_i^{\text{ilc}}(t)=\begin{cases}\boldsymbol{h}_i^{\text{ilc}*}(t-t^k), & \text{if } t\in[t^k,t^k+T]\\ 0, & \text{otherwise}\end{cases} \tag{5}$$

where $\boldsymbol{h}_i^{\text{ilc}*}(t)$ is a predefined signal on $[0,\ T]$. Therefore, $\boldsymbol{Ch}_i^{\text{ilc}}(t)$ at each trial $[t^k,\ t^k+T]$ denotes the above mentioned repetitive trajectory in the leader coordinate system. Properly defining $\boldsymbol{h}_i^{\text{ilc}*}(t)$ gives rise to various rotation behaviors of the followers around the leader to capture specific needs of the formation tasks (please see Eq. (47) as an example of predefining $\boldsymbol{h}_i^{\text{ilc}*}(t)$). The relationship among $\boldsymbol{y}_0(t)$, $\boldsymbol{Ch}_i^{\text{aoc}}(t)$ and $\boldsymbol{Ch}_i^{\text{ilc}}(t)$ is further described in Fig. 2 for a straightforward illustration. Physically, in multi-vehicle systems, by setting the output matrix $\boldsymbol{C}$, $\boldsymbol{Ch}_i(t)$ can denote the desired relative position between the leader and the follower i in which the state consists of position, velocity, and acceleration.

According to the linearity within system dynamics Eq. (1), the trajectory $\boldsymbol{y}_i(t)$ obtained using the input signal $\boldsymbol{u}_i(t)$ can be considered as the hybrid combination of two independent trajectories $\boldsymbol{Cx}_i^{\text{aoc}}(t)$ and $\boldsymbol{Cx}_i^{\text{ilc}}(t)$ obtained from the input signals $\boldsymbol{u}_i^{\text{aoc}}(t)$ and $\boldsymbol{u}_i^{\text{ilc}}(t)$ generated by AOC and ILC respectively, which satisfy $\boldsymbol{u}_i(t)=\boldsymbol{u}_i^{\text{aoc}}(t)+\boldsymbol{u}_i^{\text{ilc}}(t)$. Denote the AOC-FT error (fixed shape FT error) for each follower $i, i\in I_1^N$ along the whole task horizon as

$$\boldsymbol{e}_i^{\text{aoc}}(t)=\boldsymbol{Cx}_i^{\text{aoc}}(t)-\boldsymbol{y}_0(t)-\boldsymbol{Ch}_i^{\text{aoc}}(t),\ t\in[0,+\infty) \tag{6}$$

Also, denote the FT error as

$$\boldsymbol{e}_i(t)=\begin{cases}\boldsymbol{Cx}_i^{\text{ilc}}(t)-\boldsymbol{Ch}_i^{\text{ilc}}(t)+\boldsymbol{e}_i^{\text{aoc}}(t), & t\in[t^k,t^k+T]\\ \boldsymbol{e}_i^{\text{aoc}}(t), & \text{otherwise}\end{cases} \tag{7}$$

During the ILC initial condition resetting period, the repetitive component $\boldsymbol{h}_i^{\text{ilc}}(t)$ is set to zero and thus, ILC does not need to work, i.e., $\boldsymbol{u}_i^{\text{ilc}}(t)=0$ if $t\notin[t^k,t^k+T]$ as shown in Fig. 1. In this case, $\boldsymbol{e}_i(t)$ equals $\boldsymbol{e}_i^{\text{aoc}}(t)$ directly as shown in Eq. (7). One can see from Eq. (4) and Eq. (6) that the FT error $\boldsymbol{e}_i(t)$ satisfies

$$\boldsymbol{e}_i(t)=\boldsymbol{y}_i(t)-\boldsymbol{y}_0(t)-\boldsymbol{Ch}_i(t), t\in[0,+\infty) \tag{8}$$

In this paper, another different real leader–follower formation control mechanism is proposed by adopting AOC and ILC. The non-repetitive trajectory can be handled by AOC along the task horizon. During the ILC initial condition resetting periods (t^k+T,t^{k+1}) shown in Fig. 1, AOC makes $\boldsymbol{e}_i^{\text{aoc}}(t)$ bounded such that the ILC initial state condition is within an acceptable range for ILC implementation. As a result, ILC can deal with the repetitive trajectory to further improve the repetitive FT performance at trials $[t^{k+1},t^{k+1}+T]$. Note that the shape rotation performance is realized differently from the research.[11,13,20] Based on the above control design, the FT problem can be formulated as follows.

Definition 1. FT Problem: Given system dynamics Eq. (1), a digraph $\mathscr{G}$, for any random initial conditions $\boldsymbol{x}_i(0), i\in I_0^N$ and a bounded leader state $\boldsymbol{x}_0(t)$, design a fully distributed algorithm to provide the input signals $\boldsymbol{u}_i^{\text{aoc}}(t)$ (based on AOC controller) and $\boldsymbol{u}_i^{\text{ilc}}(t)$ (based on ILC controller) such that for each follower i, $i \in I_1^N$, the AOC-FT error $\boldsymbol{e}_i^{\text{aoc}}(t)$ in Eq. (6) is bounded along the whole task horizon and that the FT error $\boldsymbol{e}_i(t)$ in Eq. (7) is smaller than the corresponding $\boldsymbol{e}_i^{\text{aoc}}(t)$ at trial number k: $[t^k, t^k+T]$ in average, i.e.,

$$\frac{1}{T}\int_0^T \| \boldsymbol{e}_i(t^k+\tau) \|^2 \mathrm{d}\tau \leqslant \frac{1}{T}\int_0^T \| \boldsymbol{e}_i^{\text{aoc}}(t^k+\tau) \|^2 \mathrm{d}\tau \tag{9}$$

Definition 1 splits the task objective into two parts: (A) design the input signal $\boldsymbol{u}_i^{\text{aoc}}(t)$ using AOC to achieve the AOC-FT objective (time-invariant formation) such that $\boldsymbol{e}_i^{\text{aoc}}(t)$ is bounded along the task horizon; (B) design the input signal $\boldsymbol{u}_i^{\text{ilc}}(t)$ using ILC to further improve the FT performance (rotation around the leader) as shown in Eq. (9) at trials $[t^k, t^k+T]$. The controller designs of these two parts are discussed in the next two sections.

3.2. AOC for non-repetitive trajectory

In this subsection, $t \in [0, +\infty)$, and thus, t is omitted in this section only for brevity of presentation, when there is no confusion. The problem investigated in this section is stated as below.

Problem 1. Given system Eq. (1) and a digraph $\mathscr{G}$, when the leader's state $\boldsymbol{x}_0(t)$ is bounded, design an AOC controller to guarantee the boundedness of $\boldsymbol{e}_i^{\text{aoc}}(t)$ in Eq. (6) for any initial conditions $\boldsymbol{x}_i(0)$, $i \in I_0^N$.

3.2.1. AOC controller design

For an AOC controller, u_i^{aoc} is designed based on the formation shape format Eq. (3) which is time-varying. Since AOC is used in this paper for time-invariant formation control, $\boldsymbol{K}_1$ is computed as

$$\boldsymbol{A} + \boldsymbol{B}\boldsymbol{K}_1 = \boldsymbol{0} \tag{10}$$

and thus, Eq. (3) changes to $\dot{\boldsymbol{h}}_i(t) = 0$, meaning the relative vector $\boldsymbol{h}_i(t)$ from the leader to follower i is constant. Here, we set $\boldsymbol{h}_i^{\text{aoc}}(t) := \boldsymbol{h}_i(t)$ when $\dot{\boldsymbol{h}}_i(t) = 0$, which also means

$$\dot{\boldsymbol{h}}_i^{\text{aoc}}(t) = 0 \tag{11}$$

Also, a distributed adaptive observer $\boldsymbol{v}_i \in \mathbb{R}^n$ is the other key component of the AOC controller $\boldsymbol{u}_i^{\text{aoc}}$. Define the following variables for designing $\boldsymbol{u}_i^{\text{aoc}}$ of follower i

$$\tilde{\boldsymbol{x}}_i = \boldsymbol{x}_i^{\text{aoc}} - \boldsymbol{h}_i^{\text{aoc}} - \boldsymbol{x}_0 \tag{12}$$

$$\boldsymbol{\zeta}_i = \sum_{j \in \mathscr{N}_i} a_{ij}\left(\boldsymbol{x}_i^{\text{aoc}} - \boldsymbol{x}_j^{\text{aoc}} - \boldsymbol{h}_i^{\text{aoc}} + \boldsymbol{h}_j^{\text{aoc}}\right) + a_{i0}\left(\boldsymbol{x}_i^{\text{aoc}} - \boldsymbol{x}_0 - \boldsymbol{h}_i^{\text{aoc}}\right) \tag{13}$$

$$\bar{\boldsymbol{v}}_i = \sum_{j \in \mathscr{N}_i} a_{ij}(\boldsymbol{v}_i - \boldsymbol{v}_j) + a_{i0}\boldsymbol{v}_i \tag{14}$$

$$\psi_i = \bar{\boldsymbol{v}}_i - \boldsymbol{\zeta}_i, i \in I_1^N \tag{15}$$

where $\boldsymbol{\zeta}_i$ and $\bar{\boldsymbol{v}}_i$ are synthesized signals with information from neighbors. From Eq. (6) and Eq. (12), one can see that $\boldsymbol{C}\tilde{\boldsymbol{x}}_i = \boldsymbol{e}_i^{\text{aoc}}$. Denote $\boldsymbol{\psi} = [\psi_1^{\text{T}}, \psi_2^{\text{T}}, \ldots, \psi_N^{\text{T}}]^{\text{T}}$. It naturally follows that $\boldsymbol{\zeta}_i = \sum_{j=1}^N l_{ij}\tilde{\boldsymbol{x}}_j$, $\bar{\boldsymbol{v}}_i = \sum_{j=1}^N l_{ij}\boldsymbol{v}_j$ and

$$\boldsymbol{\psi} = (\mathscr{L}_1 \otimes \boldsymbol{I}_n)(\boldsymbol{v} - \tilde{\boldsymbol{x}}) \tag{16}$$

The AOC controller to solve Problem 1 is proposed as

$$\begin{cases} \boldsymbol{u}_i^{\text{aoc}} = \boldsymbol{K}_1\boldsymbol{h}_i^{\text{aoc}} + \boldsymbol{K}_2\boldsymbol{v}_i \\ \dot{\boldsymbol{v}}_i = (\boldsymbol{A} + \boldsymbol{B}\boldsymbol{K}_2)\boldsymbol{v}_i + \boldsymbol{F}(\mathrm{c}_i + \mathrm{x}_i)\left(\boldsymbol{C}\bar{\boldsymbol{v}}_i - \boldsymbol{C}\boldsymbol{\zeta}_i\right) - \boldsymbol{B}\alpha z(\eta_i) \\ \dot{c}_i = \left(\bar{\boldsymbol{v}}_i - \boldsymbol{\zeta}_i\right)^{\text{T}}\boldsymbol{C}^{\text{T}}\boldsymbol{C}\left(\bar{\boldsymbol{v}}_i - \boldsymbol{\zeta}_i\right) - \chi_i(\mathrm{c}_i - \beta_1),\ i \in I_1^N \end{cases} \tag{17}$$

where $\chi_i > 0, \beta_1 \geqslant 1$ are constants, $\alpha > 0, \boldsymbol{F} \in \mathbb{R}^{n \times q}$ are to be decided, and $\xi_i = \psi_i^{\text{T}}\boldsymbol{P}\psi_i, \eta_i = \boldsymbol{B}^{\text{T}}\boldsymbol{P}\psi_i$ with the matrix $\boldsymbol{P} \succ 0$ being a solution to the following Linear Matrix Inequality (LMI)

$$\boldsymbol{P}\boldsymbol{A} + \boldsymbol{A}^{\text{T}}\boldsymbol{P} + \mu\boldsymbol{P} - 2\boldsymbol{C}^{\text{T}}\boldsymbol{C} \prec 0 \tag{18}$$

where $\mu > 1$ is a constant to be decided. Note that the adaptive variable c_i is the time-varying coupling weight associated with follower i with $\mathrm{c}_i(0) \geqslant \beta_1$. The non-linear function $z(\cdot)$ is defined as

$$z(\boldsymbol{x}) = \begin{cases} \frac{\boldsymbol{x}}{\|\boldsymbol{x}\|} & ,\text{if } \| \boldsymbol{x} \| > \sigma_{\mathrm{i}} \\ \frac{\boldsymbol{x}}{\sigma_i} & ,\text{if } \| \boldsymbol{x} \| \leqslant \sigma_{\mathrm{i}} \end{cases} \tag{19}$$

where $\sigma_i > 0$ is the sliding-mode surface function parameter inspired from the sliding-mode control.

From Eq. (16), since $\mathscr{L}_1$ is a non-singular M-matrix from Assumption 3, $\boldsymbol{v}(t)$ will converge to $\tilde{\boldsymbol{x}}(t)$ as $t \to \infty$ if $\lim_{t\to\infty} \varrho(t) = 0$. So v_i in Eq. (17) is designed to estimate $\tilde{\boldsymbol{x}}_i$ in Eq. (12), and then is used to construct $\boldsymbol{u}_i^{\text{aoc}}$ in Eq. (17).

Remark 1. From Eq. (13) and Eq. (17), one can see clearly the control input requires both $\boldsymbol{h}_i^{\text{aoc}}$ and $\boldsymbol{h}_j^{\text{aoc}}$. The proposed AOC approach is cooperative. From the term $a_{i0}(\boldsymbol{x}_i^{\text{aoc}} - \boldsymbol{x}_0 - \boldsymbol{h}_i^{\text{aoc}})$ in Eq. (13) one can verify that not all followers need to know the leader's information.

3.2.2. AOC controller stability analysis

The following theorem is presented to illustrate the boundedness of $\tilde{\boldsymbol{x}}_i$, and then $\boldsymbol{e}_i^{\text{aoc}}$ based on $\boldsymbol{e}_i^{\text{aoc}} = \boldsymbol{C}\tilde{\boldsymbol{x}}_i, i \in I_1^N$. Denote $\boldsymbol{e}^{\text{aoc}} = [(\boldsymbol{e}_1^{\text{aoc}})^{\text{T}}, (\boldsymbol{e}_2^{\text{aoc}})^{\text{T}}, \ldots, (\boldsymbol{e}_N^{\text{aoc}})^{\text{T}}]^{\text{T}}$.

Theorem 1. Suppose Assumptions 1, 2 and 3 hold. Problem 1 is solved by the AOC controller Eq. (17) if $\boldsymbol{A} + \boldsymbol{B}\boldsymbol{K}_2$ is Hurwitz, $\alpha \geqslant \delta, \boldsymbol{F} = -\boldsymbol{P}^{-1}\boldsymbol{C}^{\text{T}}$ with $\boldsymbol{P}$ satisfying LMI, Eq. (18) and μ is designed as $\mu = \bar{\mu} + 2\kappa_1$, with $0 < \kappa_1 \leqslant \min_{i \in I_1^N}\chi_i/2, \bar{\mu} > 0$ in (A16). Then, c_i is bounded and

$$\|\boldsymbol{e}^{\text{aoc}}\| \leqslant \phi \tag{20}$$

where the upper bound ϕ is given by

$$\phi = \gamma \| \boldsymbol{I}_N \otimes \boldsymbol{C} \| \| \boldsymbol{B}\boldsymbol{K}_2 \| \| \mathscr{L}_1^{-1} \| \sqrt{\frac{2\Xi}{\underline{\mu}\lambda_{\min}(\bar{\boldsymbol{G}})\lambda_{\min}(\boldsymbol{P})}} + \gamma \| \boldsymbol{I}_N \otimes \boldsymbol{C} \| \| \boldsymbol{I}_N \otimes \boldsymbol{B} \| \sqrt{N}\delta \tag{21}$$

with $\bar{\boldsymbol{G}}$ defined in Lemma Eq. (A1), Ξ in Eq. (A10), and γ in Eq. (A21).

Proof. See Appendix A.

In Theorem 1, the condition $\alpha \geqslant \delta$ requires each follower to know the upper bound of the leader's input signal in Assumption 2. In order to relax this constraint, another observer $\hat{\delta}_i \in \mathbb{R}$ can be designed to estimate δ as follows:

$$\dot{\hat{\delta}}_i = -\bar{\delta}_i \tag{22}$$

$$\bar{\delta}_i = \sum_{j\in\mathcal{N}_i} a_{ij}(\hat{\delta}_i - \hat{\delta}_j) + a_{i0}(\hat{\delta}_i - \delta) \tag{23}$$

where $a_{i0} = 1$ means follower i needs the information of δ from the leader via the communication network, i.e., not all followers need the δ information. Denote the corresponding estimation error as $\tilde{\delta}_\iota = \hat{\delta}_\iota - \delta, \hat{\boldsymbol{\delta}} = [\hat{\delta}_1, \hat{\delta}_2, \ldots, \hat{\delta}_N]^{\mathrm{T}}$, based on $\dot{\delta}(t) = 0$ as δ is a constant, one can verify $\dot{\tilde{\delta}} = -(\mathcal{L}_1 \otimes I)\tilde{\delta}$. Since $\mathcal{L}_1$ is a positive definite matrix from Assumption 3, $\lim_{t\to\infty} \tilde{\delta}(t) = 0$ is obtained, i.e., $\lim_{t\to\infty} \hat{\delta}_i(t) = \delta$. Then, one can substitute condition $\alpha \geqslant \delta$ as $\alpha_i \geqslant \hat{\delta}_i$ and further deduce the upper bound of $\hat{\delta}_i(t)$ is $e^{-t}\sqrt{2\sum_{i=1}^{N}\tilde{\delta}_i^2(0)/N}$ based on the comparison theorem of ordinary differential equations. Note that the design of the asymptotic observer Eq. (22) is partially inspired from the work.[47] The proof to deduce the boundedness of AOC-FT error $\boldsymbol{e}_i^{\mathrm{aoc}}$ utilizing Eq. (22) with $\alpha_i \geqslant \hat{\delta}_i$ is trivial and is omitted here.

How to use the asymptotic observer (22) practically in reality One approach could be that each agent selects a large value of α_i at the beginning, and then, decreases its value gradually but keeps $\alpha_i \geqslant \hat{\delta}_i$.

Since $\lim_{t\to\infty} \hat{\delta}_i(t) = \delta$ for the asymptotic observer Eq. (22), if one needs to finalize the value of α_i quickly, i.e., in finite time, a finite-time observer $\hat{\delta}_i(t)$ is needed for each agent. Thus, a finite-time observer is constructed as follows:

$$\dot{\hat{\delta}}_i = -\frac{1}{\sum_{j=0,j\neq i}^{N} a_{ij}}\left(k|\bar{\delta}_i|^{\kappa}\mathrm{sign}\bar{\delta}_i - \sum_{j=1,j\neq i}^{N} a_{ij}\dot{\hat{\delta}}_j\right) \tag{24}$$

where $\bar{\delta}_i$ is defined in Eq. (23) and $k > 0, \kappa \in (0,1)$ are constant parameters related to the settling time T. The proof of $\lim_{t\to T} \hat{\delta}_i(t) = \delta$ can be found.[46] By using this finite-time observer, each agent can gradually obtain an appropriate value of α_i when $t \geqslant T$. By the use of the observer $\hat{\delta}_i$, the proposed AOC controller Eq. (17) is fully distributed.

4. Performance improvement based on ILC

4.1. ILC for repetitive trajectories

In this subsection, to further improve the AOC-FT performance at trials $[t^k, t^k + T]$, $k = 0, 1, \ldots, n$ as shown in Fig. 1, the technique of ILC is used to improve the repetitive FT performance (shape rotation and translation) based on the AOC-FT performance (shape translation). An ILC paradigm is first introduced, and an ILC law is proposed to compute the input signal during ILC trials. Moreover, the FT error in Eq. (7) is proved to reduce monotonically along the trial to a certain accuracy level, and a discussion is made to achieve the objective in Definition 1. To distinguish from the time $t \in [0, +\infty)$, τ is used in this section to denote the time within the interval $[0, T]$ for each ILC trial.

4.1.1. An ILC paradigm

Unlike the mechanism of AOC, ILC employs the information of the current trial to compute the input signal of the next trial. By learning from the past information of repetitive tasks, ILC is capable of improving its tracking performance and outperforming other non-ILC formation approaches in terms of tracking accuracy. Therefore, for the ILC design, the corresponding input, output and error signals are linked to the signals $\boldsymbol{u}_i^{\mathrm{ilc},k}$, $\boldsymbol{y}_i^{\mathrm{ilc},k}$, $\boldsymbol{e}_i^{\mathrm{aoc},k}$ and $\boldsymbol{e}_i^k$ defined as

$$\begin{cases} \boldsymbol{u}_i^{\mathrm{ilc},k}(\tau) = \boldsymbol{u}_i^{\mathrm{ilc}}(t^k + \tau) \\ \boldsymbol{y}_i^{\mathrm{ilc},k}(\tau) = \boldsymbol{C}\boldsymbol{x}_i^{\mathrm{ilc}}(t^k + \tau) \\ \boldsymbol{e}_i^{\mathrm{aoc},k}(\tau) = \boldsymbol{e}_i^{\mathrm{aoc}}(t^k + \tau) \\ \boldsymbol{e}_i^k(\tau) = \boldsymbol{e}_i(t^k + \tau),\ \tau \in [0, T] \end{cases} \tag{25}$$

for each follower i at trial number k. In addition, a reference signal $\boldsymbol{r}_i$ in the leader coordinate system is defined as

$$\boldsymbol{r}_i(\tau) = \boldsymbol{C}\boldsymbol{h}_i^{\mathrm{ilc}*}(\tau), \tau \in [0, T] \tag{26}$$

The above signals belong to the input and output Hilbert spaces $L_2^p[0, T]$ and $L_2^q[0, T]$, i.e.

$$\boldsymbol{u}_i^{\mathrm{ilc},k} \in L_2^p[0, T],\ \boldsymbol{y}_i^{\mathrm{ilc},k}, \boldsymbol{e}_i^{\mathrm{aoc},k}, \boldsymbol{e}_i^k, \boldsymbol{r}_i \in L_2^q[0, T] \tag{27}$$

and these spaces are defined with inner products and associated induced norms as

$$\begin{cases} \langle \boldsymbol{u}, \boldsymbol{v}\rangle_{\boldsymbol{R}} = \int_0^T \boldsymbol{u}^{\mathrm{T}}(\tau)\boldsymbol{R}\boldsymbol{v}(\tau)\mathrm{d}\tau, \|\ \boldsymbol{u}\ \|_{\boldsymbol{R}} = \sqrt{\langle \boldsymbol{u}, \boldsymbol{u}\rangle_{\boldsymbol{R}}} \\ \langle \boldsymbol{y}, \boldsymbol{z}\rangle_{\boldsymbol{Q}} = \int_0^T \boldsymbol{y}^{\mathrm{T}}(\tau)\boldsymbol{Q}\boldsymbol{z}(\tau)\mathrm{d}\tau, \|\ \boldsymbol{y}\ \|_{\boldsymbol{Q}} = \sqrt{\langle \boldsymbol{y}, \boldsymbol{y}\rangle_{\boldsymbol{Q}}} \end{cases}$$

where $\boldsymbol{R} \in \mathbb{R}^{p\times p}$ and $\boldsymbol{Q} \in \mathbb{R}^{q\times q}$ are positive definite matrices (not necessarily symmetric).

From the definitions of the component $\boldsymbol{h}_i^{\mathrm{ilc}}$ in Eq. (5) and the FT error in Eq. (7) at trial $[t^k, t^k + T]$, the above signals satisfy the following equation

$$\boldsymbol{e}_i^k = \boldsymbol{y}_i^{\mathrm{ilc},k} - \boldsymbol{r}_i + \boldsymbol{e}_i^{\mathrm{aoc},k} \tag{28}$$

Note that the relationship between $\boldsymbol{u}_i^{\mathrm{ilc},k}$ and $\boldsymbol{y}_i^{\mathrm{ilc},k}$ at trial number k can be represented in an abstract operator form as $\boldsymbol{y}_i^{\mathrm{ilc},k} = \boldsymbol{G}\boldsymbol{u}_i^{\mathrm{ilc},k}$, where the convolution operator $\boldsymbol{G} : L_2^p[0, T] \to L_2^q[0, T]$ maps $\boldsymbol{u}_i^{\mathrm{ilc},k}$ in the input space to $\boldsymbol{y}_i^{\mathrm{ilc},k}$ in the output space. According to the state space form Eq. (1), this mapping has the following form as

$$(\boldsymbol{G}\boldsymbol{u}_i^{\mathrm{ilc,k}})(\tau) = \int_0^\tau \boldsymbol{C}\mathrm{e}^{\boldsymbol{A}(\tau-s)}\boldsymbol{B}\boldsymbol{u}_i^{\mathrm{ilc},k}(s)\mathrm{d}s \tag{29}$$

Following above notations, the ILC design objective is described as: iteratively update the input signal using an ILC law

$$\boldsymbol{u}_i^{\mathrm{ilc},k+1} = \mathcal{F}(\boldsymbol{u}_i^{\mathrm{ilc},k}, \boldsymbol{e}_i^k, \boldsymbol{G}) \tag{30}$$

from the initial value $\boldsymbol{u}_i^{\mathrm{ilc},0}$, such that the desired objective Eq. (9) at trial $[t^k, t^k + T]$ is satisfied after a sufficient number of trials.

4.1.2. A norm optimal ILC law

To design an appropriate ILC law Eq. (30), the norm optimal ILC framework[48] is considered to employ the following cost function

$$\| \boldsymbol{e}_i^{k+1} \|_Q^2 + \| \boldsymbol{u}_i^{\mathrm{ilc},k+1} - \boldsymbol{u}_i^{\mathrm{ilc},k} \|_R^2 \tag{31}$$

into our ILC design, which involves two parts: the FT error and the ILC input difference between adjacent trials (trial number k and $k+1$). By optimizing this cost function, we can make the best effort to reduce the FT error while preserving a minimum change of the ILC input signal for robustness concerns. The exact values of the matrices R and Q are determined based on the weightings of the error reduction as well as robustness. Therefore, using Eq. (28), Eq. (29) and Eq. (31), a modified norm optimal problem for follower i, $i \in I_1^N$ is formulated as

$$\min_{\boldsymbol{u}}\{\| \boldsymbol{e} \|_Q^2 + \| \boldsymbol{u} - \boldsymbol{u}_i^{\mathrm{ilc},k} \|_R^2 : \boldsymbol{e} = \boldsymbol{y} - \boldsymbol{r}_i + \boldsymbol{e}_i^{\mathrm{aoc},k+1}, \boldsymbol{y} = \boldsymbol{G}\boldsymbol{u}\} \tag{32}$$

where the variable $\boldsymbol{u}$ denotes any feasible choice for $\boldsymbol{u}_i^{\mathrm{ilc},k+1}$. Solving Eq. (32) yields an ILC law in form of Eq. (30) as follows:

$$\boldsymbol{u}_i^{\mathrm{ilc},k+1} = \boldsymbol{u}_i^{\mathrm{ilc},k} - \boldsymbol{G}^*(\boldsymbol{I} + \boldsymbol{G}\boldsymbol{G}^*)^{-1}\boldsymbol{e}_i^k \tag{33}$$

where $\boldsymbol{I}$ denotes the identity operator and $\boldsymbol{G}^*$ is the adjoint operator of $\boldsymbol{G}$ defined by inner product

$$\langle \boldsymbol{u}, \boldsymbol{G}^*\boldsymbol{y} \rangle_R = \langle \boldsymbol{G}\boldsymbol{u}, \boldsymbol{y} \rangle_Q \tag{34}$$

According to the link Eq. (25), the input signal $\boldsymbol{u}_i^{\mathrm{ilc}}(t)$ along the task horizon associates with the computed input signal $\boldsymbol{u}_i^{\mathrm{ilc},k}(\tau)$ on each trial. Therefore, the value of $\boldsymbol{u}_i^{\mathrm{ilc}}(t)$ at the next trial should be assigned as

$$\boldsymbol{u}_i^{\mathrm{ilc}}(t^{k+1} + \tau) = \boldsymbol{u}_i^{\mathrm{ilc},k+1}(\tau), \tau \in [0, T] \tag{35}$$

once $\boldsymbol{u}_i^{\mathrm{ilc},k+1}$ is computed by the ILC law Eq. (33), whose convergence performance is stated in the following theorem.

Theorem 2. If the current trial FT error $\boldsymbol{e}_i^k$ satisfies

$$\| \boldsymbol{e}_i^k \| > \Delta_i^k, \text{with } \Delta_i^k = \frac{\| \boldsymbol{e}_i^{\mathrm{aoc},k+1} - \boldsymbol{e}_i^{\mathrm{aoc},k} \|}{1-\rho}, i \in I_1^N \tag{36}$$

where $\rho = \| (I + \boldsymbol{G}\boldsymbol{G}^*)^{-1} \|$, then the ILC law Eq. (33) monotonically reduces the FT error, i.e.,

$$\| \boldsymbol{e}_i^{k+1} \| < \| \boldsymbol{e}_i^k \| \tag{37}$$

Proof. See Appendix B.

Theorem 2 states that even though the ILC initial condition coming from the AOC-FT error $\boldsymbol{e}_i^{\mathrm{aoc},k}$ is non-zero, ILC law Eq. (33) still reduces the FT error $\boldsymbol{e}_i^k$.

Remark 2. The condition for reducing the Formation Tracking (FT) error $\boldsymbol{e}_i^k$ depends on comparing it with the difference in Adaptive Observer-based Control (AOC) FT errors from consecutive trials, $\|\boldsymbol{e}_i^{\mathrm{aoc},k+1} - \boldsymbol{e}_i^{\mathrm{aoc},k}\|$. Specifically, if the current error norm $\|\boldsymbol{e}_i^k\|$ exceeds a threshold Δ_i^k, which is determined by $\|\boldsymbol{e}_i^{\mathrm{aoc},k+1} - \boldsymbol{e}_i^{\mathrm{aoc},k}\|$ and the parameter ρ, the next trial's error norm $\|\boldsymbol{e}_i^{k+1}\|$ will be reduced. Here, Δ_i^k represents both the convergence point of the error reduction and the upper bound of the FT error.

Remark 3. The FT error is not guaranteed to converge to zero, since the AOC-FT error varies over the trials. From Eq. (36), the ILC law Eq. (33) is capable of reducing the error to a certain level of accuracy. Therefore, the appropriate matrices R and Q can be chosen to change the value of ρ to provide desired convergence rates and to adjust the upper bound Δ_i^k of the FT error. A suggested choice range for the values of R and Q based on the authors' implementation experience is

$$\frac{0.01}{\|\boldsymbol{G}\|^2} \leqslant \| \boldsymbol{Q}\boldsymbol{R}^{-1} \| \leqslant \frac{100}{\|\boldsymbol{G}\|^2} \tag{38}$$

4.1.3. Discussion on achieving the objective

From the objective Eq. (9) in Definition 1, according to Theorem 1, $\boldsymbol{e}_i^{\mathrm{aoc},k}$ must be bounded above as

$$\sum_{i=1}^{N} \| \boldsymbol{e}_i^{\mathrm{aoc},k} \|^2 \leqslant \phi^2 T \tag{39}$$

From Theorem 2, the ILC law Eq. (33) can reduce the FT error norm to a value smaller than Δik. To achieve the desired objective Eq. (9) in Definition 1, a comparison between Δik and $\| \boldsymbol{e}_i^{\mathrm{aoc},k} \|$ should be made. Intuitively, from the construction of Δ_i^k in Eq. (36), the AOC-FT errors $\boldsymbol{e}_i^{\mathrm{aoc},k}$ and $\boldsymbol{e}_i^{\mathrm{aoc},k+1}$ between adjacent trials should not change dramatically, and $1/(1-\rho)$ should not be too large.

Before solving the FT problem in Definition 1, the following lemma is needed.

Lemma 1. For any $a \in \mathbb{R}, b \in \mathbb{R}, c \in \mathbb{R}$ and $0 < c < 1$, if and only if the condition

$$\mathrm{sign}(a) = \mathrm{sign}(b), \frac{|b|}{1+c} \leqslant |a| \leqslant \frac{|b|}{1-c} \tag{40}$$

is satisfied, then,

$$\frac{|a-b|}{c} \leqslant |a| \tag{41}$$

Proof. See Appendix C

Theorem 3. Based on Theorems 1, 2 and Lemma 1, if the system Eq. (1) is output controllable, the FT error converges within the upper bound Δ_i^k at trial number $k+1$ and the AOC-FT errors between adjacent trials satisfy

$$\begin{cases} \mathrm{sign}(\boldsymbol{e}_{i,j}^{\mathrm{aoc}}(t^k + \tau)) = \mathrm{sign}(\boldsymbol{e}_{i,j}^{\mathrm{aoc}}(t^{k+1} + \tau)) \\ \frac{\left|\boldsymbol{e}_{i,j}^{\mathrm{aoc}}(t^k+\tau)\right|}{2-\rho} \leqslant \left|\boldsymbol{e}_{i,j}^{\mathrm{aoc}}(t^{k+1} + \tau)\right| \leqslant \frac{\left|\boldsymbol{e}_{i,j}^{\mathrm{aoc}}(t^k+\tau)\right|}{\rho} \end{cases} \tag{42}$$

where $\tau \in [0, T]$, ρ is defined in Theorem 2 and $\boldsymbol{e}_{i,j}^{\mathrm{aoc}}(t)$ denotes the j-th element of the vector $\boldsymbol{e}_i^{\mathrm{aoc}}(t)$, then, the FT problem in Definition 1 is solved.

Proof. See Appendix D.

Theorem 3 requires the sign of the AOC-FT errors to be the same between adjacent trials. For a known value of $\boldsymbol{e}_i^{\mathrm{aoc},k}$ at the current trial, from Eq. (42), one can see that the reduction of ρ to zero increases the allowed range of $\boldsymbol{e}_i^{\mathrm{aoc},k+1}$ at the next trial. By increasing this allowed range, the condition Eq. (42)

becomes more easily satisfied and hence the FT problem in Definition 1 can be solved. Since the value of ρ is affected by the choice of $\boldsymbol{Q}$ and $\boldsymbol{R}$, we can tune their values in the suggested range Eq. (38) to improve the ILC performance. Moreover, the value of $\left|\boldsymbol{e}_{i,j}^{\mathrm{aoc},k}(\tau)\right|$ also influences the allowed range of $\boldsymbol{e}_i^{\mathrm{aoc},k+1}$, which can be changed by tuning the parameter $\bar{\mu}$ in the AOC controller design based on the upper bound condition Eq. (21) in Theorem 1.

4.2. Links between AOC and ILC

Algorithm 1. AOC-ILC Algorithm

Input: System Dynamics $\boldsymbol{A}$, $\boldsymbol{B}$ and $\boldsymbol{C}$, initial ILC input $\boldsymbol{u}_i^{\mathrm{ilc},0}$, formation shape components $\boldsymbol{h}_i^{\mathrm{aoc}}(t)$ and $\dot{\boldsymbol{h}}_i^{\mathrm{aoc}}(t)$, ILC trial time T, initial condition resetting time $t^{k+1}-(t^k+T)$ and FT accuracy ϵ based on task requirement.
Output: AOC input $\boldsymbol{u}_i^{\mathrm{aoc}}$ and ILC input $\boldsymbol{u}_i^{\mathrm{ilc},k}$
1. Initialization set $k=0$.
2. During $[0, t^0]$, apply the AOC controller Eq. (17).
3. During ILC trial 0: $[t^0, t^0+T]$, apply the AOC controller (17) and the initial ILC input $\boldsymbol{u}_i^{\mathrm{ilc},0}$ to the system plant.
4. Record the FT error $\boldsymbol{e}_i^0$.
5. **while not** $\sum_1^N \| \boldsymbol{e}_i^k \| \leqslant \epsilon$ **do**
6. During $[t^k+T, t^{k+1}]$, apply the AOC controller (17) to obtain $\boldsymbol{u}_i^{\mathrm{aoc}}$, and use the ILC controller Eq. (33) to update the ILC input $\boldsymbol{u}_i^{\mathrm{ilc},k+1}$ for the following trial.
7. During ILC trial $k+1$: $[t^{k+1}, t^{k+1}+T]$, apply the AOC controller Eq. (17) to obtain $\boldsymbol{u}_i^{\mathrm{aoc}}$ and add ILC input $\boldsymbol{u}_i^{\mathrm{ilc},k+1}$ to the system plant.
8. Record the FT error $\boldsymbol{e}_i^{k+1}$.
9. $k=k+1$
10. **end while**.
11. **return** AOC input $\boldsymbol{u}_i^{\mathrm{aoc}}$ and ILC input $\boldsymbol{u}_i^{\mathrm{ilc},k}$.

According to the workflow in Fig. 1, the above two sections present an AOC-ILC algorithm (Algorithm 1) to achieve the translation and rotation of the formation shape. In addition to the link between AOC and ILC discussed in Theorems 2 and 3 in the previous section, there exists one more link related to the AOC formation shape design and the ILC repetitive trajectory setting. For better presenting this link between AOC and ILC, we first show the result of pure AOC (i.e., without ILC) to achieve FT. The AOC controller in Eq. (17) is used to achieve time-invariant FT with controller parameter $\boldsymbol{K}_1$ calculated in Eq. (10) for the initial condition setting of ILC. In fact, without ILC, AOC controller Eq. (17) can also achieve the translation and rotation of the formation shape with $\boldsymbol{K}_1$ calculated in Eq. (3) independently, herein we call the controller Eq. (17) with Eq. (3) pure AOC.

4.2.1. Pure AOC

For pure AOC, with the formation shape Eq. (3): $\dot{\boldsymbol{h}}_i(t)=(\boldsymbol{A}+\boldsymbol{B}\boldsymbol{K}_1)\boldsymbol{h}_i(t)$, there are two key components: $\boldsymbol{K}_1$ and $\boldsymbol{h}_i(\boldsymbol{t})$.

(1). For $\boldsymbol{K}_1$: Actually the application of $\boldsymbol{K}_1$ provides more flexibility for $\boldsymbol{h}_1(t)$. The Time-Varying Formation (TVF) shape will become the constant shape if $\boldsymbol{A}+\boldsymbol{B}\boldsymbol{K}_1=\boldsymbol{0}$ as Eq. (10) in this paper. $\boldsymbol{K}_1$ is also dispensable for MASs, e.g., by choosing $\boldsymbol{K}_1=0$, $\boldsymbol{h}_i(t)$ will be only related to each follower's system matrix $\boldsymbol{A}$, i.e., $\dot{\boldsymbol{h}}_i(t)=\boldsymbol{A}\boldsymbol{h}_i(t)$, which is a stringent condition when designing $\boldsymbol{h}_i(t)$. Above all, $\boldsymbol{K}_1$ has the function of expanding the feasible TVF shape set described by Eq. (3).

(2). For $\boldsymbol{h}_i(t)$: It is not arbitrary or random to choose the desired TVF shape $\boldsymbol{h}_i(t)$ since it must be compatible with each agent's dynamics according to Eq. (3). Any formation shape characterized by $\boldsymbol{h}_i(t)$ satisfying Eq. (3) can be achieved by the AOC controller Eq. (17) proposed in this paper. Since agent dynamics $(\boldsymbol{A},\boldsymbol{B})$ is unchangeable, designing $\boldsymbol{K}_1$ gives us a freedom to design any TVF shape characterized by $\boldsymbol{h}_i(t)$ satisfying Eq. (3).

As one can see there are two variables in Eq. (3): $\boldsymbol{K}_1$ and $\boldsymbol{h}_i(t)$, our design thought is that when the mathematical format $\boldsymbol{h}_i(t)$ is designed to represent the TVF shape first, then, $\boldsymbol{K}_1$ can be correspondingly calculated. From our previous work,[20] there is one kind of TVF shapes that can be achieved in this paper. When we design the concrete time-varying shapes, we ask the vectors $\boldsymbol{h}_i(t)$ to satisfy

$$\sum_{i=1}^N \boldsymbol{h}_i(t)=0 \tag{43}$$

With the condition Eq. (43) satisfied, based on Eq. (12), it means that the pure AOC objective is then to make the summation of $\boldsymbol{x}_i(t)$ converge to $N\boldsymbol{x}_0(t)$ and this implies that the location of the leader is inside the formation shape formed by the followers. Here, follower number N should be known in advance, which could be regarded reasonable as when we design a desired formation shape, we usually know how many agents we have, i.e., N agents.

Then, to design $\boldsymbol{h}_i(t)$ satisfying Eq. (3) and Eq. (43), the agent dynamics $(\boldsymbol{A},\boldsymbol{B})$ are required. One kind of real dynamics is that for unicycle vehicles, as both the kinematic model[49] and dynamic model[50] can be linearized to the following second-order dynamics in state-space as

$$\boldsymbol{A}=\begin{bmatrix}\boldsymbol{0}_{2\times2} & \boldsymbol{I}_2\\ \boldsymbol{0}_{2\times2} & \boldsymbol{0}_{2\times2}\end{bmatrix}, \boldsymbol{B}=\begin{bmatrix}\boldsymbol{0}_{2\times2}\\ \boldsymbol{I}_2\end{bmatrix}, n=4 \tag{44}$$

Choose $\boldsymbol{C}=[\boldsymbol{I}_2, 0_{2\times2}]$, then, $(\boldsymbol{A},\boldsymbol{B},\boldsymbol{C})$ is stabilizable and detectable. As a consequence, the TVF shape $\boldsymbol{h}_i(t)=[h_{i1}(t),h_{i2}(t),\dots,h_{in}(t)]^{\mathrm{T}}\in\mathbb{R}^n$ is proposed as

$$\begin{cases} h_{i1}=\theta\sin(\omega t+(i-1)2\pi/N)-\theta\cos(\omega t+(i-1)2\pi/N)\\ h_{i2}=2\theta\sin(\omega t+(i-1)2\pi/N)\\ h_{i3}=\theta\omega\sin(\omega t+(i-1)2\pi/N)+\theta\omega\cos(\omega t+(i-1)2\pi/N)\\ h_{i4}=2\theta\omega\cos(\omega t+(i-1)2\pi/N), i\in I_1^N \end{cases} \tag{45}$$

where $\theta\in\mathbb{R}$ denotes the formation shape amplitude and $\omega\in\mathbb{R}$ denotes the shape rotation frequency. One can verify that Eq. (45) satisfies Eq. (3) and Eq. (43).

Remark 4. There could be other concrete mathematical formats of $\boldsymbol{h}_i(t)$ different from Eq. (43) and Eq. (45) satisfying Eq. (3). Finding these is a topic for future work.

4.2.2. AOC-ILC

The control task specifications are as follows: the ILC trial duration is T, the AOC time between two consecutive ILC trials is $t^{k+1} - (t^k + T)$, the pure AOC formation shape $\boldsymbol{h}_i(t)$ of the followers in the leader coordinate system is proposed in Eq. (45). It follows from Eq. (4) that $\boldsymbol{h}_i(t)$ can be split into $\boldsymbol{h}_{\mathrm{i}}^{\mathrm{aoc}}(t)$ and $\boldsymbol{h}_i^{\mathrm{ilc}}(t)$ defined by

$$\begin{cases} h_{i1}^{\mathrm{aoc}}(t) = \theta\sin((i-1)2\pi/N) - \theta\cos((i-1)2\pi/N) \\ h_{i2}^{\mathrm{aoc}}(t) = 2\theta\sin((i-1)2\pi/N) \\ h_{i3}^{\mathrm{aoc}}(t) = 0 \\ h_{i4}^{\mathrm{aoc}}(t) = 0,\ i \in I_1^N,\ t \in [0, +\infty) \end{cases} \tag{46}$$

and

$$\begin{cases} h_{i1}^{\mathrm{ilc}^*}(\tau) = \theta\sin(\omega\tau + (i-1)2\pi/N) - \theta\cos(\omega\tau + (i-1)2\pi/N) \\ h_{i2}^{\mathrm{ilc}^*}(\tau) = 2\theta\sin(\omega\tau + (i-1)2\pi/N) - 2\theta\sin((i-1)2\pi/N) \\ h_{i3}^{\mathrm{ilc}^*}(\tau) = \theta\omega\sin(\omega\tau + (i-1)2\pi/N) + \theta\omega\cos(\omega\tau + (i-1)2\pi/N) \\ h_{i4}^{\mathrm{ilc}^*}(\tau) = 2\theta\omega\cos(\omega\tau + (i-1)2\pi/N),\ i \in I_1^N,\ \tau \in [0, T] \end{cases} \tag{47}$$

Here, the ILC trial duration T is designed as

$$T = 2\pi/\omega \tag{48}$$

where ω is from the pure AOC formation shape format Eq. (45). It is worth noting that Eq. (48) is the link between AOC formation shape design and ILC repetitive trajectory setting.

One can see for each follower i, the constant component $\boldsymbol{h}_i^{\mathrm{aoc}}(t) \in \mathbb{R}^4$ in Eq. (46) is the time-invariant (fixed) FT requirement along the task time horizon. The desired non-repetitive trajectory in the ground coordinate system is $\boldsymbol{C}\boldsymbol{h}_i^{\mathrm{aoc}}(t) + \boldsymbol{y}_0(t)$. The fully distributed AOC controller Eq. (17) is utilized to follow this desired trajectory (fixed shape translation performance). On the other hand, the time-varying component $\boldsymbol{h}_i^{\mathrm{ilc}}(t) \in \mathbb{R}^4$ defined by Eq. (5) and Eq. (47) is the repetitive tracking requirement vector during ILC trials. As can be seen from the gray curve in Fig. 2, $\boldsymbol{C}\boldsymbol{h}_i^{\mathrm{ilc}}(t)$ represents the repetitive rotation trajectory, e.g., circular or ellipse, etc. There are different mathematical formats of closed curves.

During ILC trials for $t \in [t^k, +t^k + T]$, the proposed fully distributed AOC and ILC algorithm (controllers Eq. (17) and Eq. (33) together) in this paper will achieve the repetitive rotation performance in the leader coordinate system. Outside of ILC trials, the proposed algorithm only achieves the shape translation performance for ILC initial condition resetting purpose (see Fig. 1). To sum up, AOC makes the FT error bounded to be inside the initial error requirement of ILC; at the same time, ILC can improve the FT error during the repetitive trials.

Remark 5. Compared to pure AOC, AOC-ILC can give rise to a smaller bounded FT error during ILC trials by employing ILC with tuning matrices such as $\boldsymbol{Q}$. AOC-ILC also presents an FT scenario of translation, translation-rotation, translation, translation-rotation, etc., which is different from a pure AOC scenario, which is always translation-rotation.

5. Numerical simulation

The performance of Algorithm 1 is verified in this section using a numerical simulation related to the scenario of unicycle formation. The comparison is also made with respect to the pure AOC algorithm (the term "algorithm" will be omitted when there is no confusion) to illustrate the advantage of combined AOC-ILC in terms of repetitive tracking error reduction.

5.1. Control task specifications

Choose MAS dynamics as $\theta = 10$ m, $\omega = 0.1\pi$, thus $T = 30$ s from Eq. (48), the AOC time between two consecutive ILC trials is $t^{k+1} - (t^k + T) = 15$ s, the non-zero input of the leader is $u_0(t) = [\mathrm{e}^{-t} + 1, 2 + \sin(0.5t)]^{\mathrm{T}}$, $t \in [0, +\infty)$. In this section, we set follower number $N = 6$ to demonstrate six vehicles forming a hexagon rotating around the real leader (shape rotation performance). For AOC controller Eq. (17), the parameters are set as $\beta_1 = 1, \sigma_i = 0.005$ and $\chi_i = 0.1, i \in I_1^N$. Then, from Eq. (A16), we choose $\kappa_1 = 0.02, \bar{\mu} = 2$ to get $\mu = 2.02$. The matrix $\boldsymbol{P}$ can be calculated by LMI Eq. (18) accordingly.

5.2. Simulation results

$$\| \bar{\boldsymbol{e}}_i^k \|^2 = \int_0^T \| \boldsymbol{e}_i(t^k + \tau) \|^2 \mathrm{d}\tau / T,\ i \in I_1^6$$

A total number of 30 repetitive trial is conducted using AOC-ILC with the initial ILC input $\boldsymbol{u}_i^{\mathrm{ilc},0} = \boldsymbol{0}$, and the weighting matrices are taken as $\boldsymbol{R} = \boldsymbol{I}$ and $\boldsymbol{Q} = 0.01\boldsymbol{I}$ based on Eq. (38). The mean square FT errors of AOC-ILC and pure AOC at each repetitive trial are plotted in Fig. 3 for each follower. Since the initial ILC input is taken as zero, the FT performance of AOC-ILC is not as good as that of pure AOC for the first few trials. Nevertheless, the mean square FT error of AOC-ILC declines along the trials, while the pure AOC error stays around a constant level for all trials. From Fig. 3, the AOC-ILC is able to improve the FT accuracy by around 10 times compared to pure AOC, which is an appealing property.

The AOC-FT error is shown in Fig. 4 where $e_3^{\mathrm{aoc}}(t)$ is plotted as an example, and the values of the adaptive parameters $c_i(t), i \in I_1^6$ are demonstrated in Fig. 5 where these parameters are kept bounded along the task time horizon. Theorem 1 is thus verified. One can also see that after the initial time (approximately 2 s), the sign of both $e_{3,1}^{\mathrm{aoc}}(t)$ and $e_{3,2}^{\mathrm{aoc}}(t)$ is always negative, and ρ is calculated as $\rho = 0.0015$. Therefore, it is easy to verify that the condition Eq. (42) in Theorem 3 is satisfied, and hence the FT problem in Definition 1 is guaranteed to be feasible.

To further demonstrate the comparison between the two methods, the square FT errors of the two algorithms along the time line for Agent 3 are taken as an example and plotted in Fig. 6 for a straightforward view. From this figure, the FT errors of AOC-ILC during the repetitive trials are much smaller than those of pure AOC after 3 trials. Meanwhile, during the interval $[t^k + T, t^{k+1}]$, the FT errors of both methods are

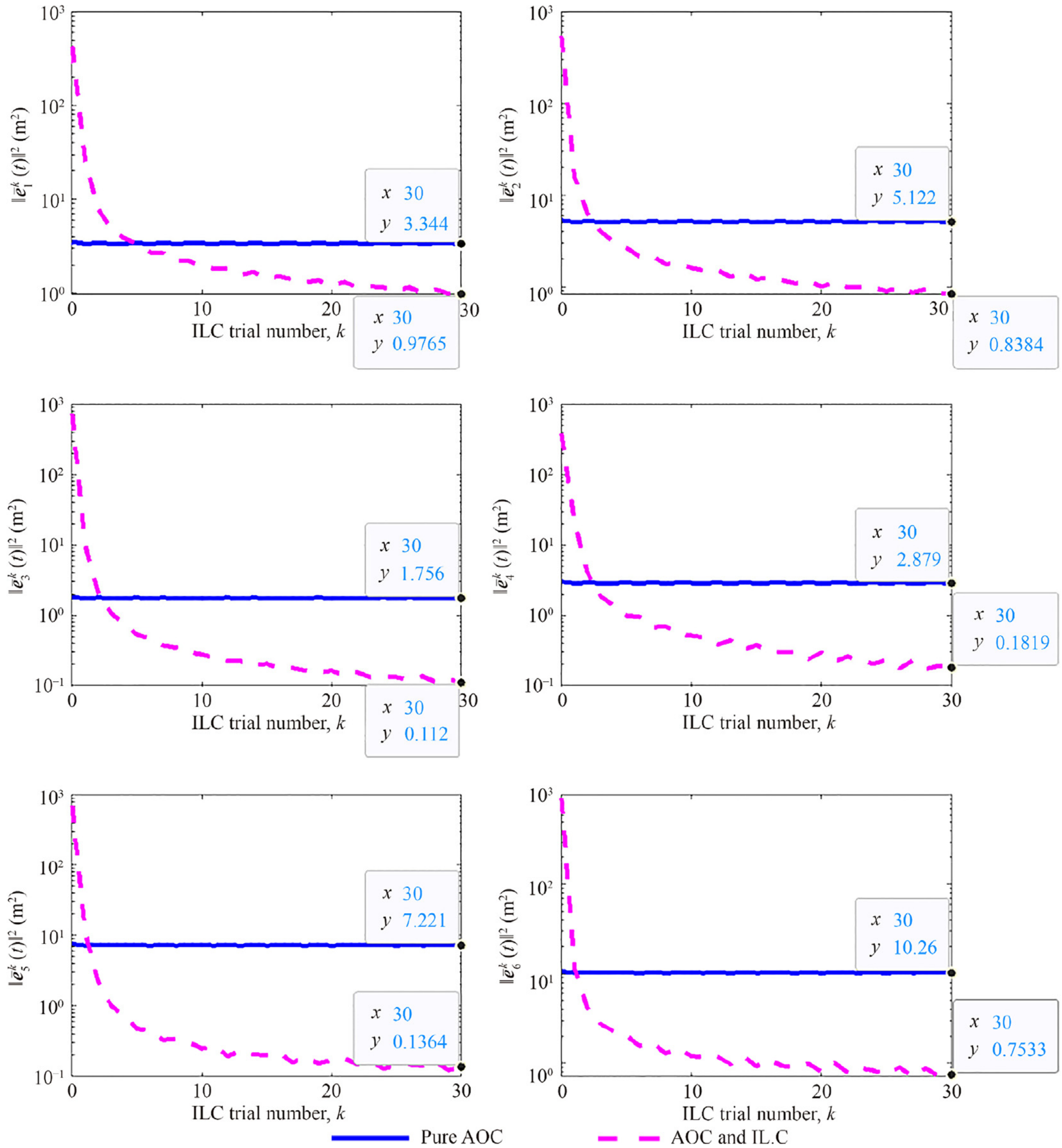

Fig. 3 Mean square formation tracking error comparison of all followers during repetitive trials.

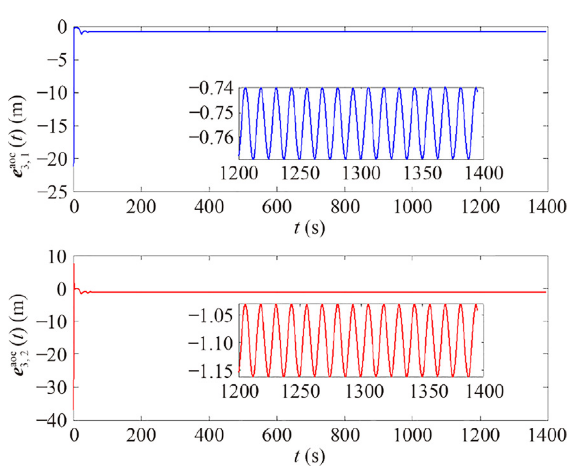

Fig. 4 Agent 3 AOC-FT error $e_i^{\mathrm{aoc}}(t)$ along the task time horizon to verify condition Eq. (42) in Theorem 3.

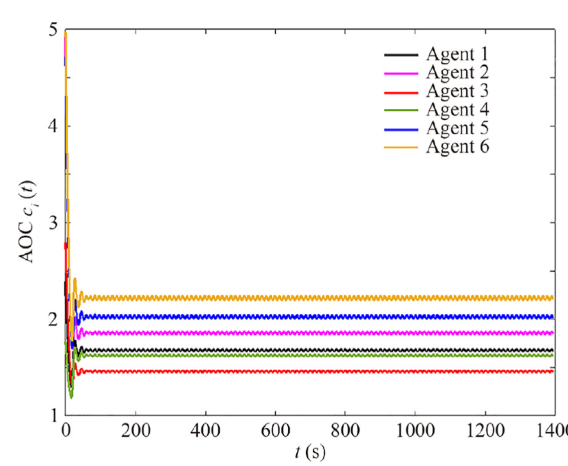

Fig. 5 Values of $c_i(t)$ in AOC-ILC along the task time horizon.

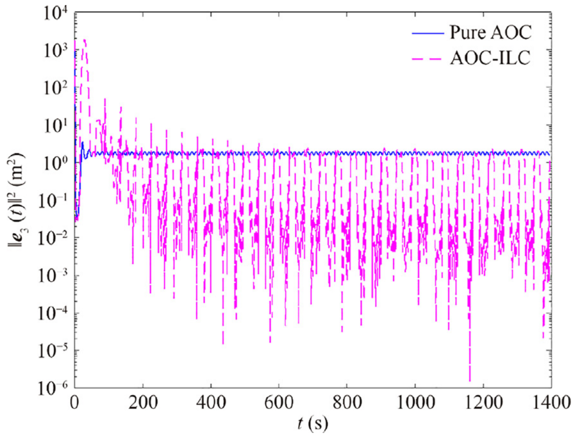

Fig. 6 Square formation tracking error comparison of Agent 3 along task time horizon.

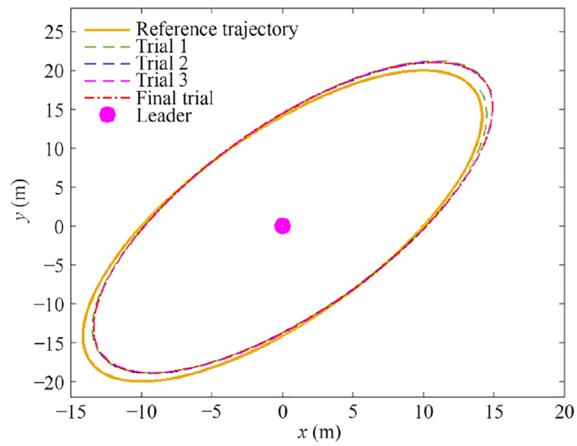

Fig. 8 Reference trajectory tracking of Agent 3 using pure AOC algorithm.

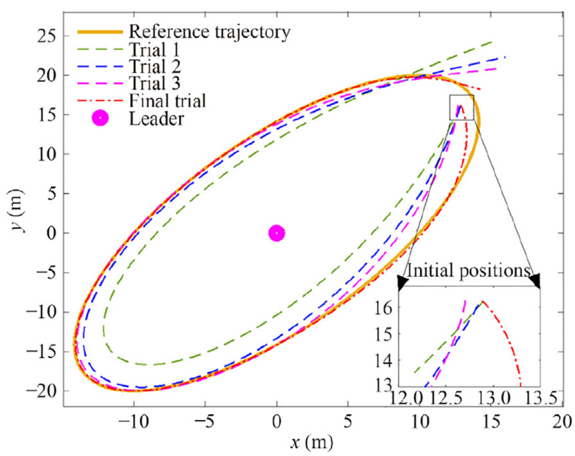

Fig. 7 Reference trajectory tracking of Agent 3 using AOC-ILC.

at a similar level. This jump phenomenon is due to the implementation of ILC during the repetitive trials, which can gradually reduce the repetitive FT error.

In addition, the reference trajectory tracking of Agent 3 in the leader coordinate system using AOC-ILC and pure AOC are respectively shown in Fig. 7 and Fig. 8. Specifically, Fig. 7 directly explains how AOC-ILC improves the repetitive FT performance along the trials. Though the initial positions are not the same as that of the reference trajectory due to the bounded AOC-FT error, AOC-ILC still makes Agent 3 track the reference trajectory well. However, as can be seen from Fig. 8, the AOC-FT error of pure AOC does not improve for all trials.

The above comparison results confirm that the proposed AOC-ILC has nice properties and can improve the FT performance during the repetitive trials comparing to pure AOC.

6. Conclusions and future work

In this paper, links between formation control and ILC with a non-repetitive real leader (non-zero input, non-repetitive trajectory) are leveraged to construct a unified framework using adaptive control and ILC. In detail, an adaptive observer-based controller is proposed to help establish an ILC controller eliminating the identical initial condition requirement. The formation tracking error during ILC trials is further reduced by the above combined algorithm. During ILC trials, the formation shape not only translates but also rotates, and a real leader exists with a non-repetitive trajectory, which are the improvements compared to existing ILC formation works, where the leader's trajectory has to be repetitive (e.g., circles) or multi-agent formation shape has to be fixed (only shape translation).

Future work will focus on discovering more formation shape mathematical formats satisfying Eq. (3) and Eq. (43) in this paper. Moreover, a rigorous robustness analysis will be conducted to check the performance of the proposed combined algorithm in the presence of model uncertainty. Meanwhile, the algorithm may be extended to handle a similar problem in non-repetitive time-varying systems.[51,52] An experimental multi-vehicle formation test platform is also under construction to validate the algorithm's practical efficacy.

CRediT authorship contribution statement

Wei JIANG: Writing – original draft, Visualization, Validation, Software, Investigation. **Yiyang CHEN:** Writing – review & editing, Writing – original draft, Funding acquisition, Formal analysis, Data curation, Conceptualization. **Hongtian CHEN:** Writing – review & editing, Resources, Project administration, Funding acquisition. **Bart De SCHUTTER:** Writing – review & editing, Supervision.

Declaration of competing interest

The authors declare that they have no known competing financial interests or personal relationships that could have appeared to influence the work reported in this paper.

Acknowledgements

This work was supported in part by the National Natural Science Foundation of China (Nos. 62103293 and 62388101), in part by the Natural Science Foundation of Jiangsu Province, China (No. BK20210709).

Appendix A.

Proof of Theorem 1. The following lemmas are needed for the Lyapunov function derivative calculation in the proof of Theorem 1.

Lemma A1. [43] (Theorem 4.25). For the non-singular M-matrix $\mathscr{L}_1$, there exists a matrix $\bar{\boldsymbol{G}} \triangleq (\operatorname{diag} g)^{-1} \succ 0$ such that $\bar{\boldsymbol{G}}\mathscr{L}_1 + \mathscr{L}_1^{\mathrm{T}}\bar{\boldsymbol{G}} \succ 0$, where $\mathrm{g} = [g_1, g_2, \ldots, g_N]^{\mathrm{T}} = \mathscr{L}_1^{-1}\mathbf{1}_N$.

Lemma A2. [53] (Young's Inequality). If the real numbers a, b, p, q satisfy $a \geqslant 0, b \geqslant 0, p > 0$ and $q > 0$ such that $1/p + 1/q = 1$, then, $ab \leqslant a^p/p + b^q/q$.

Lemma A3. [54] For a system $\dot{\boldsymbol{x}} = f(\boldsymbol{x}, t)$ where $f(\cdot)$ is locally Lipschitz in $\boldsymbol{x}$ and piecewise continuous in t, suppose that there exists a continuously differentiable function $V(\boldsymbol{x}, t) \geqslant 0$ satisfying

$$\begin{cases} \mathscr{K}_1(\| \boldsymbol{x} \|) \leqslant V(\boldsymbol{x}, t) \leqslant \mathscr{K}_2(\| \boldsymbol{x} \|) \\ \dot{V}(\boldsymbol{x}, t) \leqslant -\mathscr{K}_3(\| \boldsymbol{x} \|) + \Xi \end{cases}$$

where $\Xi > 0$ is a constant, $\mathscr{K}_1, \mathscr{K}_2$ are class $\mathscr{K}_\infty$ functions, and $\mathscr{K}_3$ is a class $\mathscr{K}$ function. Then, the solution $\boldsymbol{x}(t)$ of $\dot{\boldsymbol{x}} = f(\boldsymbol{x}, t)$ is uniformly ultimately bounded.

Lemma A4. [55] If a real function $V(t)$ satisfies $\dot{V}(t) \leqslant -aV(t) + b$, where a, b are positive constants, then

$$V(t) \leqslant \left(V(0) - \frac{b}{a}\right)\mathrm{e}^{-at} + \frac{b}{a}$$

Denote $\hat{\boldsymbol{c}} = \operatorname{diag}(c_1, c_2, \ldots, c_N), \hat{\boldsymbol{\xi}} = \operatorname{diag}(\xi_1, \xi_2, \ldots, \xi_N)$. So based on Eq. (15), Eq. (16) and Eq. (17), the dynamics of ψ and c_i are

$$\begin{cases} \dot{\boldsymbol{\psi}} = \left[\boldsymbol{I}_N \otimes \boldsymbol{A} + \mathscr{L}_1(\hat{\boldsymbol{c}} + \hat{\boldsymbol{\xi}}) \otimes \boldsymbol{FC}\right]\boldsymbol{\psi} - (\mathscr{L}_1 \otimes \boldsymbol{B})(\alpha z(\eta) - 1_N \otimes \boldsymbol{u_0}) \\ \dot{c}_i = \boldsymbol{\psi}_i^{\mathrm{T}}\boldsymbol{C}^{\mathrm{T}}\boldsymbol{C}\boldsymbol{\psi}_i - \chi_i(c_i - \beta_1), i \in I_1^N \end{cases} \tag{A1}$$

Firstly, let

$$V_1 = \frac{1}{2}\sum_{i=1}^{N}\frac{1}{g_i}\left[(2c_i + \xi_i)\xi_i + (c_i - \beta)^2\right] \tag{A2}$$

where $g_i, i \in I_1^N$ are constructed as in Lemma A1 and $\beta > 0$ is a constant to be decided later. From $\dot{c}_i(t) \geqslant 0, c_i(0) \geqslant \beta_1 \geqslant 1$, we have $c_i(t) \geqslant 1, \forall t \geqslant 0$. Note further that $\xi_i = \boldsymbol{\psi}_i^{\mathrm{T}}\boldsymbol{P}\boldsymbol{\psi}_i \geqslant 0$, so V_1 is positive definite. Then,

$$\begin{aligned} \dot{V}_1 &= \sum_{i=1}^{N}[\tfrac{1}{g_i}(c_i + \xi_i)\dot{\xi}_i + \tfrac{1}{g_i}\xi_i\dot{c}_i + \tfrac{1}{g_i}(c_i - \beta)\dot{c}_i] \\ &= \boldsymbol{\psi}^{\mathrm{T}}[\bar{\boldsymbol{G}}(\hat{c} + \hat{\xi}) \otimes (\boldsymbol{PA} + \boldsymbol{A}^{\mathrm{T}}\boldsymbol{P}) + \bar{\boldsymbol{G}}(\hat{c} + \hat{\xi} - \beta I) \otimes \boldsymbol{C}^{\mathrm{T}}\boldsymbol{C} \\ &\quad + (\hat{c} + \hat{\xi})(\bar{\boldsymbol{G}}\mathscr{L}_1 + \mathscr{L}_1^{\mathrm{T}}\bar{\boldsymbol{G}})(\hat{c} + \hat{\xi}) \otimes \boldsymbol{PFC}]\boldsymbol{\psi} + \Omega_1 \\ &\quad - \textstyle\sum_{i=1}^{N}\frac{1}{g_i}(c_i - \beta)\chi_i(c_i - \beta_1) - \sum_{i=1}^{N}\frac{1}{g_i}\xi_i\chi_i(c_i - \beta_1) \\ &\leqslant \boldsymbol{\psi}^{\mathrm{T}}[\bar{\boldsymbol{G}}(\hat{c} + \hat{\xi}) \otimes (\boldsymbol{PA} + \boldsymbol{A}^{\mathrm{T}}\boldsymbol{P}) + \bar{\boldsymbol{G}}(\hat{c} + \hat{\xi} - \beta I) \otimes \boldsymbol{C}^{\mathrm{T}}\boldsymbol{C} \\ &\quad - \lambda_0(\hat{c} + \hat{\xi})^2 \otimes \boldsymbol{C}^{\mathrm{T}}\boldsymbol{C}]\boldsymbol{\psi} + \Omega_1 + \Omega_2 \end{aligned} \tag{A3}$$

where

$$\Omega_1 = -2\boldsymbol{\psi}^{\mathrm{T}}[\bar{\boldsymbol{G}}(\hat{c} + \hat{\xi})\mathscr{L}_1 \otimes \boldsymbol{PB}](\alpha z(\eta) - 1_N \otimes u_0) \tag{A4}$$

$$\Omega_2 = -\sum_{i=1}^{N}\frac{1}{g_i}(c_i - \beta)\chi_i(c_i - \beta_1) \tag{A5}$$

and $\bar{\boldsymbol{G}} \succ 0$ are defined in Lemma A1. The inequality comes from $\bar{\boldsymbol{G}}\mathscr{L}_1 + \mathscr{L}_1^{\mathrm{T}}\bar{\boldsymbol{G}} \geqslant \lambda_0\boldsymbol{I}_N, \lambda_0 > 0$ and $\sum_{i=1}^{N}[\xi_i\chi_i(c_i - \beta_1)/g_i] \geqslant 0$ based on $c_i \geqslant \beta_1$ from (17). By using Lemma A2, we get

$$\boldsymbol{\psi}^{\mathrm{T}}[\bar{\boldsymbol{G}}(\hat{c} + \hat{\xi}) \otimes \boldsymbol{C}^{\mathrm{T}}\boldsymbol{C}]\boldsymbol{\psi} \leqslant \boldsymbol{\psi}^{\mathrm{T}}[(\frac{\lambda_0}{2}(\hat{c} + \hat{\xi})^2 + \frac{\bar{\boldsymbol{G}}^2}{2\lambda_0}) \otimes \boldsymbol{C}^{\mathrm{T}}\boldsymbol{C}]\boldsymbol{\psi}$$

Substituting the above inequality into Eq. (A3) yields

$$\begin{aligned} \dot{V}_1 \leqslant \;& \boldsymbol{\psi}^{\mathrm{T}}\{\bar{\boldsymbol{G}}(\hat{c} + \hat{\xi}) \otimes (\boldsymbol{PA} + \boldsymbol{A}^{\mathrm{T}}\boldsymbol{P}) \\ & -[\tfrac{\lambda_0}{2}(\hat{c} + \hat{\xi})^2 - \tfrac{\bar{\boldsymbol{G}}^2}{2\lambda_0} + \beta\bar{\boldsymbol{G}}] \otimes \boldsymbol{C}^{\mathrm{T}}\boldsymbol{C}\}\boldsymbol{\psi} + \Omega_1 + \Omega_2 \\ & \leqslant -\boldsymbol{\psi}^{\mathrm{T}}[\bar{\boldsymbol{G}}(\hat{c} + \hat{\xi}) \otimes \mathscr{H}]\boldsymbol{\psi} + \Omega_1 + \Omega_2 \end{aligned} \tag{A6}$$

where

$$\mathscr{H} = -(\boldsymbol{PA} + \boldsymbol{A}^{\mathrm{T}}\boldsymbol{P} - 2\boldsymbol{C}^{\mathrm{T}}\boldsymbol{C}) \tag{A7}$$

One can see $\mathscr{H} \succ \mu\boldsymbol{P} \succ 0$ from LMI Eq. (18). Given the law that $a + b \geqslant 2\sqrt{ab}, \forall a, b \in \mathbb{R}^+$, for arriving at the second inequality in Eq. (A6), we have chosen

$$\beta \geqslant \frac{5}{2\lambda_0}\max_{i \in \boldsymbol{I}_1^N}\frac{1}{g_i} \tag{A8}$$

Secondly, for the component Ω_1 inside $\dot{V}_1$, the non-linear function $z(\cdot)$ in Eq. (19) is used to deal with the leader's bounded input $u_0(t)$. Following the similar calculation steps of Eqs. (34)–(39), we have

$$\dot{V}_1 \leqslant -\frac{1}{2}\boldsymbol{\psi}^{\mathrm{T}}[\bar{\boldsymbol{G}}(\hat{c} + \hat{\xi}) \otimes \mathscr{H}]\boldsymbol{\psi} - \sum_{i=1}^{N}\frac{\chi_i}{4g_i}(c_i - \beta)^2 + \Xi \tag{A9}$$

where

$$\begin{aligned} \Xi = \;& \tfrac{(\beta - \beta_1)^2}{2}\textstyle\sum_{i=1}^{N}\frac{\chi_i}{g_i} + \sum_{i=1}^{N}\frac{\sigma_i}{g_i}[a_{i0}\delta + (2N - 1)\alpha] \\ & \cdot\left\{2\beta_1 + \sigma_i(\tfrac{4}{\chi_i} + \tfrac{2\lambda_{\max}(\boldsymbol{P})}{\lambda_{\min}(\mathscr{H})})[a_{i0}\delta + (2N - 1)\alpha]\right\} \end{aligned} \tag{A10}$$

Based on $\mathscr{H} \succ 0$ in Eq. (A7) and $\sum_{i=1}^{N}[\chi_i(c_i - \beta)^2/(4g_i)] \geqslant 0$, we get

$$\dot{V}_1 \leqslant -\frac{1}{2}\boldsymbol{\psi}^T[\bar{G}(\hat{c} + \hat{\xi}) \otimes \mathscr{H}]\boldsymbol{\psi} + \Xi \tag{A11}$$

Define the continuous function $\mathscr{K}_3(\| \boldsymbol{\psi} \|) = \boldsymbol{\psi}^{\mathrm{T}}[\bar{\boldsymbol{G}}(\hat{c} + \hat{\xi}) \otimes \mathscr{H}]\boldsymbol{\psi}$. Because $\bar{G}(\hat{c} + \hat{\xi}) \succ 0$ and $\mathscr{H} \succ 0$, it is easy to verify $\mathscr{K}_3$ is a class $\mathscr{K}$ function. Considering $\Xi > 0$, from Eq. (A11) and Lemma A3, it is easy to conclude that $\boldsymbol{\psi}(t)$, which is the solution of the nonautonomous system $\dot{\boldsymbol{\psi}} = f(\boldsymbol{\psi}, t)$ in Eq. (A1), is uniformly ultimately bounded, i.e., $\boldsymbol{\psi}$ is bounded.

Thirdly, the dynamics of $\tilde{\boldsymbol{x}}_i$ in Eq. (12) can be calculated based on Eq. (1), Eq. (11) and $\boldsymbol{u}_i^{\mathrm{aoc}}$ in (17) as $\dot{\tilde{\boldsymbol{x}}}_i = \boldsymbol{A}\tilde{\boldsymbol{x}}_i - \boldsymbol{B}u_0 + \boldsymbol{BK}_2\boldsymbol{v}_i$, which can be reformulate as

$$\dot{\tilde{\boldsymbol{x}}}_i = \tilde{\boldsymbol{A}}\tilde{\boldsymbol{x}}_i + \tilde{\boldsymbol{u}}_i, i \in I_1^N \tag{A12}$$

where $\widetilde{A} = A + BK_2$ is Hurwitz and $\widetilde{u}_i = BK_2(v_i - \widetilde{x}_i) - Bu_0$. Based on Assumption 2, u_0 is bounded. As $\mathscr{L}_1$ is non-singular, there exists $v - \widetilde{x} = (\mathscr{L}_1^{-1} \otimes I)\varrho$ from Eq. (16). Based on $\|U \otimes W\| = \|U\|\,\|W\|$ if $U \in \mathbb{R}^{n\times n}, W \in \mathbb{R}^{m\times m}$, we have

$$\|v - \widetilde{x}\| = \|\mathscr{L}_1^{-1}\|\|\psi\| \tag{A13}$$

which means $v_i - \widetilde{x}_i$ is also bounded.[56] Therefore, $\widetilde{u}_i$ is the bounded input in Eq. (A12). Based on the Input to State Stability (ISS) theory,[57] the linear system with 0-globally asymptotic stability (0-GAS) automatically satisfies the Bounded-Input Bounded-State (BIBS) property, i.e., $\widetilde{x}_i$ is bounded.

Fourthly, we come to calculate the upper bound of AOC-FT error e_i^{aoc}. Considering $\xi_i = \psi_i^{\mathrm{T}} P \psi_i \geqslant 0$ in Eq. (17), from Eq. (A2) we obtain

$$\kappa_1 V_1 \leqslant \kappa_1 \sum_{i=1}^{N} \frac{c_i + \xi_i}{g_i} \psi_i^{\mathrm{T}} P \psi_i + \sum_{i=1}^{N} \frac{\kappa_1}{2g_i}(c_i - \beta)^2 \tag{A14}$$

where $\kappa_1 > 0$ is a constant to be designed later. Combining Eq. (A9) and Eq. (A14) gives

$$\begin{aligned}\dot{V}_1 \leqslant & -\tfrac{1}{2}\psi^{\mathrm{T}}[\bar{G}(\hat{c}+\hat{\xi}) \otimes \mathscr{H}]\psi - \sum_{i=1}^{N} \tfrac{\chi_i}{4g_i}(c_i-\beta)^2 + \Xi \\ & -\kappa_1 V_1 + \kappa_1 \sum_{i=1}^{N} \tfrac{c_i+\xi_i}{g_i} \psi_i^{\mathrm{T}} P \psi_i + \sum_{i=1}^{N} \tfrac{\kappa_1}{2g_i}(c_i-\beta)^2 \\ = & -\kappa_1 V_1 - \tfrac{1}{2}\psi^{\mathrm{T}}[\bar{G}(\hat{c}+\hat{\xi}) \otimes (\mathscr{H} - 2\kappa_1 P)]\psi \\ & -\sum_{i=1}^{N} \tfrac{(\chi_i - 2\kappa_1)}{4g_i}(c_i-\beta)^2 + \Xi\end{aligned} \tag{A15}$$

Select

$$0 < \kappa_1 \leqslant \min_{i\in I_1^N} \frac{\chi_i}{2}, \mu = \bar{\mu} + 2\kappa_1, \bar{\mu} > 0 \tag{A16}$$

such that based on LMI (18), we get

$$\mathscr{H} - 2\kappa_1 P \succ (\mu - 2\kappa_1) P = \bar{\mu} P \succ 0 \tag{A17}$$

Then, we obtain

$$\dot{V}_1 \leqslant -\kappa_1 V_1 + \Xi \tag{A18}$$

In light of Lemma A4, we could deduce that V_1 exponentially converges to the residual set $\Pi = \{V_1 : V_1 < \Xi/\kappa_1\}$ with a convergence rate faster than $\mathrm{e}^{-\kappa_1 t/2}$. From Eq. (A2) and based on $c_i(t) \geqslant \beta_1 \geqslant 1$, we have $V_1 \geqslant \min_{i\in I_1^N}[\lambda_{\min}(P)\|\psi\|^2/g_i + \sum_{i=1}^{N}(c_i-\beta)^2/(2g_i)]$. Since ϱ is uniformly ultimately bounded and β in Eq. (A8) is a constant, we can conclude that $c_i, i \in I_1^N$ are uniformly ultimately bounded. Furthermore, from Eq. (A17) there is $\lambda_{\min}(\mathscr{H} - 2\kappa_1 P) > \bar{\mu}\lambda_{\min}(P)$, and thus from Eq. (A15) that if $\|\psi\|^2 > 2\Xi/(\bar{\mu}\lambda_{\min}(\bar{G})\lambda_{\min}(P))$, then $\dot{V}_1 \leqslant -\kappa_1 V_1$. Therefore, ψ satisfies

$$\|\psi\| \leqslant \sqrt{\frac{2\Xi}{\bar{\mu}\lambda_{\min}(\bar{G})\lambda_{\min}(P)}} \tag{A19}$$

Finally, since dynamics $\widetilde{x}_i$ in Eq. (A12) is ISS, $\dot{\widetilde{x}} = (I_N \otimes (A + BK_2))\widetilde{x} + \widetilde{u}$ is also ISS with $\widetilde{u} = (I_N \otimes (BK_2))(v - \widetilde{x}) - (I_N \otimes B)(1_N \otimes u_0)$. Based on the work,[57] we get

$$\|\widetilde{x}\| \leqslant \gamma \|\widetilde{u}\|_\infty \tag{A20}$$

where

$$\gamma = \int_0^\infty \|e^{s(I_N \otimes (A+BK)_2)}\| ds < \infty \tag{A21}$$

As $\|u_0\| \leqslant \delta$ from Assumption 2, based on $\|\widetilde{u}\|_\infty \leqslant \|\widetilde{u}\|$ we have

$$\begin{aligned}\|\widetilde{u}\|_\infty \leqslant \; & \|I_N \otimes (BK_2)\|\|v - \widetilde{x}\| + \|I_N \otimes B\|\,\|1_N \otimes u_0\|, \\ & \leqslant \|BK_2\|\|v - \widetilde{x}\| + \|I_N \otimes B\|\sqrt{N}\delta\end{aligned} \tag{A22}$$

From Eqs. (A13), (A19), (A20), (A22) and $C\widetilde{x}_i = e_i^{\mathrm{aoc}}$, we obtain the upper bound of e^{aoc} as in Eq. (21). In this way, Problem 1 is solved.

Appendix B. Proof of Theorem 2

It follows from Eq. (28) and Eq. (32) that

$$\begin{aligned} e_i^{k+1} &= G[u_i^{\mathrm{ilc},k} - G^*(I + GG^*)^{-1}e_i^k] - r_i + e_i^{\mathrm{aoc},k+1} \\ &= (I + GG^*)^{-1}e_i^k + e_i^{\mathrm{aoc},k+1} + Gu_i^{\mathrm{ilc},k} - r_i - e_i^k \\ &= (I + GG^*)^{-1}e_i^k + (e_i^{\mathrm{aoc},k+1} - e_i^{\mathrm{aoc},k}), i \in I_1^N \end{aligned} \tag{B1}$$

Based on Eq. (B1), there exists the inequality

$$\begin{aligned} \| e_i^{k+1} \| & \leqslant \| (I + GG^*)^{-1} \| \| e_i^k \| + \| e_i^{\mathrm{aoc},k+1} - e_i^{\mathrm{aoc},k} \| \\ & = \rho \| e_i^k \| + \| e_i^{\mathrm{aoc},k+1} - e_i^{\mathrm{aoc},k} \| \\ & \leqslant \rho \| e_i^k \| + \epsilon_i \end{aligned} \tag{B2}$$

If the condition Eq. (36) holds, one has

$$\rho\| e_i^k \| + \epsilon_i < \| e_i^k \| \tag{B3}$$

which together with the inequality Eq. (B2) gives rise to the monotonic error reduction performance Eq. (37).

Appendix C. Proof of Lemma 1

Sufficient condition. If the condition Eq. (40) is satisfied, it follows that

$$\frac{b}{1+c} \leqslant a \leqslant \frac{b}{1-c} \tag{C1}$$

and the inequality Eq. (41) becomes

$$a \leqslant \frac{b}{1-c} \tag{C2}$$

for $a \geqslant b$, $a \geqslant 0$ and $b \geqslant 0$. It is clear that this inequality holds in this case. We can also obtain

$$\frac{b}{1+c} \leqslant a \tag{C3}$$

for $a < b$, $a \geqslant 0$ and $b \geqslant 0$, and the inequality Eq. (41) holds. By symmetry, the inequality Eq. (41) holds when a and b are both negative or zero as well. In this sense, the sufficiency of the condition Eq. (40) is proved.

Necessary condition. If the inequality Eq. (41) holds, it follows that

$$(1-c)a \leqslant b \tag{C4}$$

for $a \geqslant b$, $a \geqslant 0$ and $b \geqslant 0$, which gives rise to

$$b \leqslant a \leqslant \frac{b}{1-c} \tag{C5}$$

We can also obtain

$$\frac{b}{1+c} \leqslant a < b \tag{C6}$$

for $a < b$, $a \geqslant 0$ and $b \geqslant 0$. By symmetry, we have

$$\frac{b}{1-c} \leqslant a \leqslant \frac{b}{1+c} \tag{C7}$$

for a and b are both negative. Therefore, the above inequalities at specific cases yield the condition Eq. (40), which proves its necessity.

Appendix D. Proof of Theorem 3

According to the work,[58] since the system Eq. (1) is output controllable, the eigenvalues of the self-adjoint operator $\boldsymbol{G}\boldsymbol{G}^*$ are all positive according to the definitions of the convolution operator $\boldsymbol{G}$ and its adjoint operator $\boldsymbol{G}^*$ in Eq. (29) and Eq. (34). It follows that

$$\langle \boldsymbol{y}, \boldsymbol{G}\boldsymbol{G}^*\boldsymbol{y}\rangle = \| \boldsymbol{G}^*\boldsymbol{y} \|^2 \geqslant \underline{\lambda}^2 \| \boldsymbol{y} \|^2 \tag{D1}$$

where $\underline{\lambda}^2$ is the smallest eigenvalue of $\boldsymbol{G}\boldsymbol{G}^*$ and it is positive as well. Adding $\langle \boldsymbol{y}, \boldsymbol{y}\rangle$ at both sides of the above inequality yields

$$\langle \boldsymbol{y}, (\boldsymbol{I} + \boldsymbol{G}\boldsymbol{G}^*)\boldsymbol{y}\rangle = \| \boldsymbol{y} \| \| (\boldsymbol{I} + \boldsymbol{G}\boldsymbol{G}^*)\boldsymbol{y} \| \geqslant (1 + \underline{\lambda}^2) \| \boldsymbol{y} \|^2 \tag{D2}$$

Therefore, $\| (I + \boldsymbol{G}\boldsymbol{G}^*) \| \geqslant 1 + \underline{\lambda}^2$, and

$$\rho = \| (I + \boldsymbol{G}\boldsymbol{G}^*)^{-1} \| \leqslant \frac{1}{1 + \underline{\lambda}^2} < 1 \tag{D3}$$

Given the condition Eq. (42) is satisfied and $0 < \rho < 1$, according to Lemma 1, we have

$$\frac{\left| e^{aoc}_{i,j}(t^{k+1} + \tau) - e^{aoc}_{i,j}(t^k + \tau) \right|}{1 - \rho} \leqslant \left| e^{aoc}_{i,j}(t^{k+1} + \tau) \right| \tag{D4}$$

In addition, based on the 2-norm of a signal,[59] $\Delta\, ik$ in Theorem 2 can be computed as

$$\Delta\, ik = \frac{1}{1-\rho} \sqrt{\int_0^T \sum_{j=1}^{q} (e^{aoc}_{i,j}(t^{k+1} + \tau) - e^{aoc}_{i,j}(t^k + \tau))^2 \mathrm{d}\tau} \tag{D5}$$

which gives rise to the inequality

$$\begin{aligned} \Delta\, ik &\leqslant \sqrt{\textstyle\int_0^T \sum_{j=1}^{q} (e^{aoc}_{i,j}(t^{k+1} + \tau))^2 \mathrm{d}\tau} \\ &= \sqrt{\textstyle\int_0^T \| \boldsymbol{e}^{\mathrm{aoc}}_i(t^{k+1} + \tau) \|^2 \mathrm{d}\tau} \end{aligned} \tag{D6}$$

Recall in Theorem 2 that $\Delta\, ik$ is the upper bound of the FT error, i.e. $\| \boldsymbol{e}^{k+1}_i \| \leqslant \Delta\, ik$.

Similar to Eq. (D5), $\| \boldsymbol{e}^{k+1}_i \|$ is computed as

$$\| \boldsymbol{e}^{k+1}_i \| = \sqrt{\int_0^T \| \boldsymbol{e}_i(t^{k+1} + \tau) \|^2 \mathrm{d}\tau} \tag{D7}$$

Therefore, from Eq. (D6) and Eq. (D7), the desired objective Eq. (9) in Definition 1 can be achieved at trial number $k + 1$.

References

1. Zhou PP, Chen BM. Semi-global leader-following consensus-based formation flight of unmanned aerial vehicles. *Chin J Aeronaut* 2022;**35**(1):31–43.
2. Wu T, Wang J, Tian BL. Periodic event-triggered formation control for multi-UAV systems with collision avoidance. *Chin J Aeronaut* 2022;**35**(8):193–203.
3. Zhang XZ, Zhang F, Huang PF. Formation planning for tethered multirotor UAV cooperative transportation with unknown payload and cable length. *IEEE Trans Autom Sci Eng* 2024;**21**(3):3449–60.
4. Zhou YM, Yang F, Zhang CY, et al. Cooperative decision-making algorithm with efficient convergence for UCAV formation in beyond-visual-range air combat based on multi-agent reinforcement learning. *Chin J Aeronaut* 2024;**37**(8):311–28.
5. Zhang XZ, Yang QK, Xiao F, et al. Linear formation control of multi-agent systems. *Automatica* 2025;**171**:111935.
6. Scardovi L, Sepulchre R. Synchronization in networks of identical linear systems. *Automatica* 2009;**45**(11):2557–62.
7. Schenato L, Fiorentin F. Average TimeSynch: a consensus-based protocol for clock synchronization in wireless sensor networks. *Automatica* 2011;**47**(9):1878–86.
8. Oh KK, Park MC, Ahn HS. A survey of multi-agent formation control. *Automatica* 2015;**53**:424–40.
9. Liu YF, Liu JJ, He ZP, et al. A survey of multi-agent systems on distributed formation control. *Unmanned Syst* 2024;**12**(5):913–26.
10. Cao L, Cheng ZJ, Liu Y, et al. Event-based adaptive NN fixed-time cooperative formation for multiagent systems. *IEEE Trans Neural Netw Learn Syst* 2024;**35**(5):6467–77.
11. Dong XW, Hu GQ. Time-varying formation control for general linear multi-agent systems with switching directed topologies. *Automatica* 2016;**73**:47–55.
12. Jiang W, Wen GG, Peng ZX, et al. Fully distributed formation-containment control of heterogeneous linear multiagent systems. *IEEE Trans Autom Control* 2019;**64**(9):3889–96.
13. Briñón-Arranz L, Seuret A, Canudas-de-Wit C. Cooperative control design for time-varying formations of multi-agent systems. *IEEE Trans Autom Control* 2014;**59**(8):2283–8.
14. Antonelli G, Arrichiello F, Caccavale F, et al. Decentralized time-varying formation control for multi-robot systems. *Int J Robot Res* 2014;**33**(7):1029–43.
15. Jiang W, Liu K, Charalambous T. Multi-agent consensus with heterogeneous time-varying input and communication delays in digraphs. *Automatica* 2022;**135**:109950.
16. Liu TF, Jiang ZP. Distributed formation control of nonholonomic mobile robots without global position measurements. *Automatica* 2013;**49**(2):592–600.
17. Cao M, Yu CB, Anderson BDO. Formation control using range-only measurements. *Automatica* 2011;**47**(4):776–81.
18. Li ZK, Ren W, Liu XD, et al. Distributed consensus of linear multi-agent systems with adaptive dynamic protocols. *Automatica* 2013;**49**(7):1986–95.
19. Jiang W, Peng ZX, Rahmani A, et al. Distributed consensus of linear MASs with an unknown leader *via* a predictive extended state observer considering input delay and disturbances. *Neurocomputing* 2018;**315**:465–75.
20. Jiang W. A unified framework of fully distributed time-varying formation control for large-scale multi-agent systems: an observer viewpoint, *2019 18th European control conference*. Piscataway: IEEE Press; 2019.
21. Bristow D, Tharayil M, Alleyne A. A survey of iterative learning control. *IEEE Control Syst. Mag* 2006;**26**(3):96–144.
22. Arimoto S, Kawamura S, Miyazaki F. Bettering operation of robots by learning. *J Robotic Syst* 1984;**1**(2):123–40.

23. Chen YY, Chu B, Freeman CT. Point-to-point iterative learning control with optimal tracking time allocation. *IEEE Trans Control Syst Technol* 2018;**26**(5):1685–98.
24. Bu XH, Liang JQ, Hou ZS, et al. Data-driven terminal iterative learning consensus for nonlinear multiagent systems with output saturation. *IEEE Trans Neural Netw Learn Syst* 2021;**32**(5):1963–73.
25. Freeman CT, Tan Y. Iterative learning control with mixed constraints for point-to-point tracking. *IEEE Trans Control Syst Technol* 2013;**21**(3):604–16.
26. Chen YY, Chu B, Freeman CT. A coordinate descent approach to optimal tracking time allocation in point-to-point ILC. *Mechatronics* 2019;**59**:25–34.
27. Oomen T, Rojas CR. Sparse iterative learning control with application to a wafer stage: Achieving performance, resource efficiency, and task flexibility. *Mechatronics* 2017;**47**:134–47.
28. Chen YY, Chu B, Freeman CT. Iterative learning control for robotic path following with trial-varying motion profiles. *IEEE/ASME Trans Mechatron* 2022;**27**(6):4697–706.
29. Steinhauser A, Swevers J. An efficient iterative learning approach to time-optimal path tracking for industrial robots. *IEEE Trans Ind Inform* 2018;**14**(11):5200–7.
30. Chen YY, Freeman CT. Iterative learning control for piecewise arc path tracking with validation on a gantry robot manufacturing platform. *ISA Trans* 2023;**139**:650–9.
31. Chen YY, Wang YM, Freeman CT. Iterative learning control of minimum energy path following tasks for second-order MIMO systems: an indirect reference update framework. *IEEE Trans Cybern* 2025;**55**(7):3403–16.
32. Shen D, Zhang W, Wang YQ, et al. On almost sure and mean square convergence of P-type ILC under randomly varying iteration lengths. *Automatica* 2016;**63**:359–65.
33. Hoelzle DJ, Barton KL. On spatial iterative learning control *via* 2-D convolution: stability analysis and computational efficiency. *IEEE Trans Control Syst Technol* 2016;**24**(4):1504–12.
34. Hao SL, Liu T, Rogers E. Extended state observer based indirect-type ILC for single-input single-output batch processes with time- and batch-varying uncertainties. *Automatica* 2020;**112**:108673.
35. Freeman C. Introduction. *Control system design for electrical stimulation in upper limb rehabilitation*. Cham: Springer International Publishing; 2015. p. 1–5.
36. Ahn HS, Chen Y. Iterative learning control for multi-agent formation. *2009 ICCAS-SICE*. Piscataway: IEEE Press; 2009.
37. Liu Y, Jia YM. An iterative learning approach to formation control of multi-agent systems. *Syst Control Lett* 2012;**61**(1):148–54.
38. Bu XH, Cui LZ, Hou ZS, et al. Formation control for a class of nonlinear multiagent systems using model-free adaptive iterative learning. *Int J Robust Nonlinear Control* 2018;**28**(4):1402–12.
39. Meng DY, Jia YM, Du JP, et al. On iterative learning algorithms for the formation control of nonlinear multi-agent systems. *Automatica* 2014;**50**(1):291–5.
40. Hui Y, Chi RH, Huang B, et al. 3-D learning-enhanced adaptive ILC for iteration-varying formation tasks. *IEEE Trans Neural Netw Learn Syst* 2020;**31**(1):89–99.
41. Meng DY. Convergence conditions for solving robust iterative learning control problems under nonrepetitive model uncertainties. *IEEE Trans Neural Netw Learn Syst* 2019;**30**(6):1908–19.
42. Jin X. Nonrepetitive leader–follower formation tracking for multiagent systems with LOS range and angle constraints using iterative learning control. *IEEE Trans Cybern* 2019;**49**(5):1748–58.
43. Qu Z. *Cooperative control of dynamical systems: Applications to autonomous vehicles*. Berlin: Springer; 2009. p. 168–9.
44. Wang D, Wang Z, Chen MF, et al. Distributed optimization for multi-agent systems with constraints set and communication time-delay over a directed graph. *Inf Sci* 2018;**438**:1–14.
45. Zuo S, Song YD, Lewis FL, et al. Time-varying output formation containment of general linear homogeneous and heterogeneous multiagent systems. *IEEE Trans Control Netw Syst* 2019;**6**(2):537–48.
46. Hua YZ, Dong XW, Hu GQ, et al. Distributed time-varying output formation tracking for heterogeneous linear multiagent systems with a nonautonomous leader of unknown input. *IEEE Trans Autom Control* 2019;**64**(10):4292–9.
47. Cai H, Lewis FL, Hu GQ, et al. The adaptive distributed observer approach to the cooperative output regulation of linear multi-agent systems. *Automatica* 2017;**75**:299–305.
48. Amann N, Owens DH, Rogers E. Iterative learning control using optimal feedback and feedforward actions. *Int J Control* 1996;**65**(2):277–93.
49. Cepeda-Gomez R, Perico LF. Formation control of nonholonomic vehicles under time delayed communications. *IEEE Trans Autom Sci Eng* 2015;**12**(3):819–26.
50. Lawton JRT, Beard RW, Young BJ. A decentralized approach to formation maneuvers. *IEEE Trans Robot Autom* 2003;**19**(6):933–41.
51. Chen YY, Jiang W, Charalambous T. Machine learning based iterative learning control for non-repetitive time-varying systems. *Int J Robust Nonlinear Control* 2023;**33**(7):4098–116.
52. Wang L, Huangfu ZW, Li RW, et al. Iterative learning control with parameter estimation for non-repetitive time-varying systems. *J Frankl Inst* 2024;**361**(3):1455–66.
53. Bernstein DS. *Matrix mathematics: Theory, facts, and formulas*. Princeton: Princeton University Press; 2009. p. 36.
54. Corless M, Leitmann G. Continuous state feedback guaranteeing uniform ultimate boundedness for uncertain dynamic systems. *IEEE Trans Autom Control* 1981;**26**(5):1139–44.
55. Khalil HK. *Noninear systems*. New Jersey: Prentice Hall; 1996. p. 111–81.
56. Laub AJ. *Matrix analysis for scientists and engineers*. Philadelphia: Society for Industrial and Applied Mathematics; 2004. p. 139–44.
57. Sontag ED. *Nonlinear and optimal control theory*. Berlin: Springer; 2008. p. 163–220.
58. Owens DH, Freeman CT, Van Dinh T. Norm-optimal iterative learning control with intermediate point weighting: Theory, algorithms, and experimental evaluation. *IEEE Trans Control Syst Technol* 2013;**21**(3):999–1007.
59. Doyle JC, Francis BA, Tannenbaum AR. *Feedback control theory*. New York: Courier Corporation; 2013. p. 13–24.